Autoantibodies targeting CRB2 and Nephrin correlate with extrafollicular B cells in idiopathic podocytopathies

Tho-Alfakar Al-Aubodah* [1,2,3,4], Simon Leclerc* [2,3,4,5], Lamine Aoudjit[3,4], Ratna Samanta[4], Cherry Mammen[6], Allison Dart[7], Anne-Laure Lapeyraque[8], Catherine Morgan[9], Mallory L. Downie[10], Kunimasa Yan[11], Satoka Mori[12], Susan M. Samuel[6], Ciriaco A. Piccirillo** [1,2,5], Tomoko Takano** [3,4,5]

*Co-first author
**Co-senior author

[1] Department of Microbiology & Immunology, Faculty of Medicine and Health Sciences, McGill University, McGill University, Montréal, Québec, Canada
[2] Infectious Diseases and Immunity in Global Health Program, Research Institute of the McGill University Health Centre, Montréal, Québec, Canada
[3] Metabolic Disorders and Complications Program, Research Institute of the McGill University Health Centre, Montréal, Québec, Canada
[4] Department of Medicine, Division of Nephrology, Research Institute of the McGill University Health Centre, Montréal, Québec, Canada
[5] Department of Experimental Medicine, Faculty of Medicine and Health Sciences, McGill University, McGill University, Montréal, Québec, Canada
[6] Department of Pediatrics, Division of Nephrology, Faculty of Medicine, University of British Columbia, Vancouver, British Columbia, Canada
[7] Department of Pediatrics and Child Health, Division of Nephrology, University of Manitoba, Winnipeg, Manitoba, Canada
[8] Department of Pediatrics, Division of Nephrology, Université de Montréal, Montréal, Québec, Canada
[9] Department of Pediatrics, Division of Nephrology, University of Alberta, Edmonton, Alberta, Canada
[10] Department of Pediatrics, Division of Nephrology, Research Institute of the McGill University Health Centre, Montréal, Québec, Canada
[11] Department of Pediatrics, Division of Nephrology, Kyorin University School of Medicine, Tokyo, Japan
[12]Diagnostics Research Department, Life Innovation, Denka Co., Ltd, Machida City, Tokyo, Japan

Keywords: podocytopathy, idiopathic nephrotic syndrome, minimal change disease, focal segmental glomerulosclerosis, autoantibodies, CRB2, Nephrin, B cells, autoimmunity

Correspondence:
Tomoko Takano, M.D., Ph.D.
Research Institute of the McGill University Health Centre
1001 Boulevard Décarie, Montréal, Québec H4A 3J1, Canada
Bloc E, EM1.3244
E-mail: tomoko.takano@mcgill.ca

ABSTRACT

The recent discovery of autoantibodies against slit diaphragm proteins in idiopathic podocytopathies suggest an etiology of podocyte-directed autoimmunity. However, the immune mechanisms underlying the heterogeneity in disease phenotypes remain unknown. By examining the autoantibody and B cell profiles of children and adults with idiopathic podocytopathies, we identify anti-CRB2 as a prevalent autoantibody across disease phenotypes, with preferential accumulation in adults. Anti-CRB2 can occur alongside anti-Nephrin in humans, and mouse models showing epitope spreading as a potential mechanism for their emergence. In children, both autoantibodies correlated with T-bet^{+} CD21^{low} atypical B cell expansion in blood. In adults, elevated frequencies of classical memory B cells indicated a greater degree of B cell dysregulation than in children. Further profiling in children revealed a broadly dysregulated B cell pool poised for activation and the preferential accumulation of V_H4-39^{+} B cell clonotypes within the repertoire. These findings provide rationale for the heterogeneity in idiopathic podocytopathies and highlights the importance of identifying biomarkers for advancing care.

INTRODUCTION

Podocytopathies are kidney diseases characterized by severe cytoskeletal derangements in podocytes, the primary filtering cells of the glomerulus, leading to massive proteinuria and the development of nephrotic syndrome (Anders et al., 2023; Kopp et al., 2020). Although autoantibodies against podocyte antigens are the established causative agents of one such podocytopathy – namely, membranous nephropathy – they were only recently discovered in the class of idiopathic podocytopathies (Beck et al., 2009; Hengel et al., 2024; Watts et al., 2022). Idiopathic podocytopathies include the clinical diagnosis of idiopathic nephrotic syndrome (INS) in non-biopsied children encompassing both steroid-sensitive (SSNS) and steroid-resistant (SRNS) forms, as well as the histological diagnoses of minimal change disease (MCD) and primary focal segmental glomerulosclerosis (FSGS) in children and adults who have undergone a biopsy (Al-Aubodah et al., 2025; D'Agati et al., 2011; Vivarelli et al., 2023). Unlike the autoantibodies found in membranous nephropathy, which target podocyte antigens at the subepithelial interface with the glomerular basement membrane, the autoantibodies found in idiopathic podocytopathies mostly target proteins of the slit diaphragm, the primary structure responsible for glomerular filtration, including Nephrin, NEPH1, and Podocin (Beck et al., 2009; Hengel et al., 2024; Raglianti et al., 2025; Watts et al., 2022). The presence of these autoantibodies across all forms of idiopathic podocytopathy supports the emerging concept that these pathologies exist, at least in part, on a shared disease spectrum ranging from no or minimal fibrosis that frequently responds to steroid treatment, a phenotype characteristic of childhood disease (e.g. MCD or FSGS tip variant), to significant glomerular scarring that often resists steroids and will eventually require dialysis and transplantation, a presentation more prevalent in adults (e.g. FSGS collapsing variant) (Maas et al., 2016). Nevertheless, distinct anti-slit

diaphragm autoantibody species are variably present amongst patients. Consequently, characterizing the autoantibody landscape in idiopathic podocytopathies is essential for understanding disease pathogenesis and heterogeneity.

The pathogenic potential of anti-slit diaphragm autoantibodies can be inferred from their presence along podocytes in biopsies from seropositive individuals and by the general success of B cell-depletion at maintaining long-term disease remission (Raglianti et al., 2024; Ravani et al., 2016; Sinha and Bagga, 2013; Watts et al., 2022). Specifically, anti-Nephrin seropositivity is associated with heavier proteinuria and its presence is associated with post-transplant recurrence of MCD/FSGS (Batal et al., 2024; Hengel et al., 2024; Shirai et al., 2024; Watts et al., 2022). Indeed, immunizing mice with Nephrin drives autoantibody production and the development of nephrotic syndrome (Hengel et al., 2024). With growing interest in autoreactivity towards other slit diaphragm proteins, we recently reported that immunization with Crumbs cell polarity complex 2 (CRB2), a transmembrane protein that maintains Nephrin positioning at the slit diaphragm, induces anti-CRB2 autoantibody and results in nephrotic syndrome in mice (Hada et al., 2022; Möller-Kerutt et al., 2021). Notably, CRB2 mutations are known to cause congenital nephrotic syndrome, highlighting its importance in glomerular filtration (Slavotinek et al., 2015). Despite their proven pathogenicity in mice, autoantibodies against CRB2 have yet to be identified in humans.

The immune mechanisms driving the emergence of anti-slit diaphragm autoantibodies in human disease also remain undefined. We recently demonstrated that children with INS have an enlarged pool of T-bet^{+} CD21^{low} atypical B cells (atBCs), a B cell population known to be enriched with autoreactive clones and commonly expanded following acute viral infections, chronic parasitic infections, and autoimmunity (Al-Aubodah et al., 2023; Ambegaonkar et al.,

2022). Unlike classical memory B cells (cMBCs), which are defined as $CD27^+$ $CD21^+$ B cells that give rise to long-lived plasma cells via germinal center reactions in B cell follicles, atBCs arise extrafollicularly and rapidly convert into short-lived plasmablasts to provide an immediate source of antibodies (Elsner and Shlomchik, 2020). These extrafollicular responses are linked with autoantibody generation in various systemic autoimmune diseases, with the abundance of atBCs in peripheral blood often correlating with autoantibody titers, like in systemic lupus erythematosus (Ambegaonkar et al., 2022; He and Vinuesa, 2024; Jenks et al., 2019; Jenks et al., 2018). Importantly, it remains to be determined whether these extrafollicular responses are a consistent feature across idiopathic podocytopathies, and whether they are involved in emergence of anti-slit diaphragm-autoantibodies.

In this study, we examine the relationship between anti-slit diaphragm autoantibodies and B cell dysregulation in children and adults with idiopathic podocytopathies. We demonstrate that anti-CRB2 autoantibodies are prevalent across INS, MCD and FSGS, with higher seroprevalence, titers, and rate of co-occurrence with anti-Nephrin in affected adults than in children. We also show that T-bet$^+$ $CD21^{low}$ atBCs and short-lived plasmablasts are expanded in both children and adults, with adults exhibiting a high degree of concomitant follicular responses. In children, atBC expansion and plasmablast formation correlates with anti-slit diaphragm autoantibodies, indicating a close link between the observed B cell dysregulation and the podocyte-targeted autoantibody response. Finally, using single-cell RNA-sequencing, we show that both pre- and post-antigenic B cells from children with INS are primed for activation, leading to the generation of a B cell repertoire skewed towards autoreactivity-prone B cell receptors (BCRs). Overall, this study provides further evidence that idiopathic podocytopathies exist on a disease spectrum with anti-slit diaphragm autoantibodies and extrafollicular B cell

responses as underlying features and highlights the need for biomarkers to better understand disease heterogeneity.

RESULTS

Autoantibodies to CRB2 are prevalent in idiopathic podocytopathies.

While autoantibodies to Nephrin have been well-documented in idiopathic podocytopathies, it is unknown whether the underlying autoimmunity in these diseases extends to the closely related slit diaphragm protein CRB2. Thus, we sought to characterize the seroprevalence of anti-CRB2 autoantibodies, relative to anti-Nephrin, in a cohort of individuals with idiopathic podocytopathies (N = 82), other glomerulopathies (N = 22), and healthy controls (N = 28) (**Supplemental Table 1**). For each patient, we used the earliest available active disease serum sample to determine seropositivity. In children with idiopathic podocytopathies, anti-CRB2 IgG was detected in 9/19 patients (48%) with non-biopsied INS, 12/24 (50%) with biopsy-proven MCD and 2/8 (25%) with primary FSGS. In comparison, anti-Nephrin IgG was present in 3/19 patients (16%) with non-biopsied INS, 6/24 (25%) with biopsy-proven MCD and 4/8 (50%) with primary FSGS (**Figure 1A**). In adults, anti-CRB2 seropositivity was significantly higher than in children (27/31 [87%] adults, 23/51 [45%] children, P = 0.0002), with anti-CRB2 IgG detected in 9/10 adults (90%) with MCD and 18/21 (86%) with primary FSGS. In contrast, anti-Nephrin seropositivity was comparable between adults and children (9/31 [29%] adults, 13/51 [23%] children, P = 0.6136), with anti-Nephrin IgG present in 3/10 adults (30%) with MCD and 6/21 (29%) with primary FSGS. Only a small fraction of individuals with membranous nephropathy or other glomerulopathies were seropositive for either autoantibody, highlighting the specificity of anti-CRB2 and anti-Nephrin for INS, MCD and FSGS (**Figure 1A**).

Interestingly, subsequent relapses were not consistently associated with seropositivity for the same IgG autoantibody, indicating that the podocyte-targeted response may fluctuate or evolve over the course of disease (**Supplemental Figure 1A**). IgM and IgA isotypes of anti-

CRB2 and anti-Nephrin were also prevalent in idiopathic podocytopathies (**Supplemental Figure 1B**). Notably, of the 23 (N_{child} = 19, N_{adult} = 4) and 47 (N_{child} = 25, N_{adult} = 22) individuals lacking anti-CRB2 IgG and anti-Nephrin IgG, respectively, 13 (N_{child} = 11, N_{adult} = 2) and 14 (N_{child} = 8, N_{adult} = 6) were seropositive for IgM/IgA isotypes thereby increasing total autoantibody seropositivity.

Anti-CRB2 titers were highest in individuals with steroid-resistant forms of idiopathic podocytopathy and were, accordingly, markedly greater in adults than in children, suggesting that the accumulation of anti-CRB2 autoantibodies may depend on more sustained B cell responses (**Figure 1B, C**). Indeed, isotype-switched (IgG/IgA) anti-CRB2 autoantibodies were much more prevalent than non-switched (IgM) versions in adults (**Supplemental Figure 1B**) and seropositivity for anti-CRB2 IgG was significantly more associated with adult-onset disease (**Supplemental Figure 1C**). Co-seropositivity for both anti-CRB2 and anti-Nephrin IgG was more frequent in adults (8/31, [26%]) than in children (6/51 [12%], P = 0.1330), again suggesting a more advanced podocyte-directed B cell response in adults (**Figure 1D**).

Treatment with immunosuppressive agents was associated with a significant reduction in both anti-CRB2 and anti-Nephrin IgG titers (**Figure 1E**). In fact, most patients that were seropositive during active disease reverted to seronegative status in remission. Nevertheless, correlations between autoantibody titers and proteinuria during active disease were marginal, with only anti-Nephrin IgG seropositivity being associated with higher proteinuria, consistent with a recent report (**Supplemental Figure 1D, E**) (Hengel et al., 2024). Altogether, these findings establish anti-CRB2 as a new anti-slit diaphragm autoantibody present in idiopathic podocytopathies. Unlike anti-Nephrin autoantibodies, anti-CRB2 autoantibodies preferentially

accumulate in affected adults, suggesting an association with, and possible role in, later stages of disease progression.

Anti-CRB2 autoantibodies localize to podocytes in affected glomeruli.

To determine if anti-CRB2 autoantibodies play a role in podocytopathy, we investigated whether these autoantibodies localized with podocytes in affected individuals. Assessment of glomeruli from seven idiopathic podocytopathy patients from whom flash-frozen kidney biopsy tissue was available showed punctate IgG deposits in glomerular podocytes in all five anti-CRB2 seropositive individuals, but not the two anti-CRB2/Nephrin seronegative individuals (**Figure 1F, Supplemental Figure 1F, Supplemental Table 1**). Consistently, overall IgG staining intensity was higher in glomeruli of anti-CRB2 seropositive patients than seronegative ones (**Figure 1G**). High resolution microscopy of a donor seropositive for both anti-CRB2 and anti-Nephrin showed that IgG overlapped with both CRB2 and Nephrin independently, thus confirming the presence of both autoantibodies along the podocytes (**Figure 1H**). Though CRB2 and Nephrin were often co-localized, we observed greater IgG co-localization with CRB2 than Nephrin **(Figure 1I)**. These data underline a possible role for anti-CRB2 autoantibodies in mediating the podocytopathy observed in these diseases.

Anti-slit diaphragm autoantibodies can arise through epitope spreading.

The close spatial relationship between Nephrin and CRB2 at the slit diaphragm along with the co-occurrence of autoantibodies against these antigens, particularly in adults with idiopathic podocytopathies, suggests that loss of tolerance to slit diaphragm proteins may occur through epitope spreading, the process by which the scope of an immune response gradually

expands to recognize additional epitopes on the same antigen or on adjacent autoantigens (Vanderlugt and Miller, 2002). To test this, we immunized mice with a portion of the extracellular domains of either mouse Crb2 ($Crb2_{601-940}$) or Nephrin ($Nephrin_{384-731}$) and re-challenged them at 14 and 28 days following initial immunization to induce podocytopathy (**Figure 1J**). $Crb2_{601-940}$-immunized mice developed significant proteinuria by 6-weeks after initial immunization, whereas $Nephrin_{384-731}$-immunized mice developed milder proteinuria that emerged by 12-weeks (**Figure 1K**). As expected, both groups generated robust autoantibody responses to the immunizing antigen (**Figure 1L**). Strikingly, we also observed significant induction of autoantibodies against the non-immunizing antigen in both settings (**Figure 1L**). Thus, epitope spreading may contribute to the loss of tolerance to slit diaphragm proteins.

Atypical B cell expansion is a salient feature of B cell dysregulation in idiopathic podocytopathies.

To characterize the B cell landscape underlying the generation of anti-slit diaphragm autoantibodies, we profiled peripheral blood B cells in children and adults with idiopathic podocytopathies by multi-parametric flow cytometry (**Supplemental Table 1, Supplemental Figure 2A**). Frequencies of naïve B cells were diminished in both children and adults, though at distinct developmental stages: children exhibited a selective decrease in pre-splenic transitional B cells, whereas adults had fewer post-splenic mature B cells compared to healthy controls (**Figure 2A, B, Supplemental Figure 2B**). In adults, we saw a concomitant increase in cMBCs, a follicular B cell population that remained unchanged in children (**Figure 2C**).

$CD21^{low}$ B cells, a B cell population associated with B cell dysregulation in autoimmune diseases and immunodeficiencies, were expanded in children and adults with idiopathic

podocytopathies in comparison to controls, though this expansion was more prominent in adults (**Figure 2D**). These cells predominantly retained an IgD^+ IgM^+ profile and expressed the transcription factor T-bet, consistent with an extrafollicular atBC phenotype (**Figure 2E, F**). Indeed, frequencies of T-bet^+ $CD21^{low}$ atBCs were significantly elevated in both children with INS and adults with MCD/FSGS, establishing atBC expansion as a shared feature of B cell dysregulation across pediatric and adult forms of idiopathic podocytopathies (**Figure 2G, Supplemental Figure 2B**). Although atBCs in systemic lupus erythematosus are often identified with double-negative (DN, IgD^- $CD27^-$) and DN2 ($CXCR5^{low}$ $CD21^{low}$) cells, these subsets were not enriched in our cohort (**Supplemental Figure 2C**) (Jenks et al., 2019). Instead, most atBCs in idiopathic podocytopathies retained surface IgD expression, suggesting they emerged from recent activation. Consistently, the DN2 B cell precursor population, termed activated naïve (aNAV, IgD^+ $CD27^-$ $CXCR5^{low}$ $CD21^{low}$), was significantly expanded in adults (**Supplemental Figure 2C**).

Supporting the involvement of extrafollicular responses in idiopathic podocytopathies, plasmablasts ($CD20^-$ $CD19^+$) were markedly expanded in both children and adults (**Figure 2H, Supplemental Figure 2B**). These cells were preferentially IgD^+, consistent with an extrafollicular origin (**Figure 2I**). While plasmablasts were characteristically proliferative in all individuals, active plasmablast expansion was more pronounced in children (**Figure 2J**). Together, these findings point to a profoundly dysregulated B cell landscape in idiopathic podocytopathies characterized by a contraction of the naïve compartment and the induction of prominent extrafollicular responses (**Figure 2K**).

Atypical B cells are associated with anti-slit diaphragm autoantibodies in children.

To investigate whether the observed B cell derangements were associated with the emergence of anti-slit diaphragm autoantibodies, we examined correlations between peripheral B cell subsets and autoantibody titers in individuals from whom both peripheral blood mononuclear cell (PBMC) and serum samples were obtained at the same blood draw (N_{child} = 26, N_{adult} = 17). In affected children, frequencies of T-bet^{+} CD21^{low} atBCs correlated significantly with titers of both anti-CRB2 and anti-Nephrin IgG (**Figure 3A**). This correlation improved when considering the combined seroreactivity to both antigens. Although total plasmablast frequencies did not correlate with autoantibody titers, stratifying plasmablasts by IgM/IgD expression revealed that isotype-switched plasmablasts were significantly associated with anti-Nephrin IgG titers (**Figure 3B**). This correlation was close to significance with anti-CRB2 IgG titers and improved when co-seropositivity for both autoantibodies was considered. In contrast, no significant correlations were observed in adults with idiopathic podocytopathies (**Supplemental Figure 3A, B**). These findings suggest that the podocyte-directed autoantibody response, at least in children, is linked to extrafollicular B cell responses.

B cells from children with INS display heightened activation states.

Given the strong association between B cell dysregulation and autoantibody production in children, we hypothesized that the B cell compartment in this group may reflect an early stage in the pathogenesis of idiopathic podocytopathies, offering a valuable opportunity to study the breakdown of tolerance to podocyte antigens. To this end, we conducted single-cell RNA-sequencing for gene expression and V(D)J repertoire profiling on mature (CD10^{-}) B cells isolated from peripheral blood of eight children with INS, three age-matched healthy controls, and one child with a non-glomerular atopic disease as a disease control (**Supplemental Table 1**).

Following quality control, we retained 118,706 B cells (93,766 from INS; 24,310 from controls) with expression data, of which 88,334 cells (69,843 from INS; 18,491 from controls) had paired V(D)J sequences (**Supplemental Figure 4A, B**). Data integration and clustering yielded 11 distinct B cell clusters (**Figure 4A, Supplemental Data 1**). These included five naïve clusters (B0, B1, B3, B4, B9) characterized by high *BACH2* and *IL4R* expression, one of which (B4) still retained *NEIL1*-expressing transitional naïve cells despite prior depletion of $CD10^+$ cells (**Figure 4B, Supplemental Figure 4C**). Five clusters (B2, B5, B6, B7, B8) expressed transcripts associated with memory B cells like *BCL2A1*, *TNFRSF13B*, and *IGHA1*, and one cluster (B10) corresponded to plasmablasts based on *PRDM1*, *JCHAIN*, and *XBP1* expression (**Figure 4B, Supplemental Figure 4C**). Notably, two clusters showed prominent activation signatures: naïve cluster B3 (naïve-act) and memory cluster B7 (actMBC), both expressing high levels of *CD69*, *FOSB*, and *NR4A1* (**Figure 4B, Supplemental Figure 4C**). The expansion of these activated B cells represented the most striking difference in comparison to control children (**Figure 4C**).

Memory clusters were further divided into extrafollicular memory B cells (B2, B8) and follicular cMBCs (B5, B6). Cluster B2 resembled marginal zone (MZ) B cells defined by high expression of *CD1C*, *TNFRSF13B*, and *CD24*, and unmutated IgM BCRs (**Figure 4B, D, Supplemental Figure 4C**) (Al-Aubodah et al., 2023; Siu et al., 2022; Tull et al., 2021). Cluster B8 corresponded with atBCs given their highly characteristic transcriptional profile (*FCRL5*, *FGR*, *ENC1*, *ITGAX*, etc.), low levels of somatic hypermutation, and limited class-switching, mainly to IgG1 (**Figure 4B, D, Supplemental Figure 4C**) (Holla et al., 2021; Sutton et al., 2021). In contrast, clusters B5 and B6 displayed higher rates of somatic hypermutation and class-switching, consistent with cMBCs that have undergone germinal center reactions (**Figure 4B, D**). While both B5 and B6 were thus termed switched memory (SM) B cells, B6 showed greater

rates of isotype-switching and expressed high levels of *TNFRSF13B* (TACI) and was therefore distinguished as SM-TACI B cells (**Figure 4B, D**).

To further resolve perturbations in B cell states in INS, we used miloR to identify the specific B cell neighbourhoods within each cluster that are differentially abundant between INS and controls (**Figure 4E**) (Dann et al., 2022). Notably, B cell neighbourhoods enriched in INS were broadly distributed across clusters – except plasmablasts – suggesting a widespread derangement of the B cell compartment. In particular, neighbourhoods associated with activated B cell states (B3, B7) were strongly enriched in INS consistent with the general expansion of these clusters as noted above (**Figure 4E**). Additionally, MZ-like B cells (B2) and atBCs (B8) accounted for most the INS-associated neighbourhoods within the memory B cell pool, corresponding with a shift toward extrafollicular B cell activation. In contrast, neighbourhoods enriched in controls were almost exclusively present within naïve clusters (**Figure 4E**). Altogether, the increased abundance of activated B cells and the bias towards extrafollicular memory B cell phenotypes point to extrafollicular B cell activation as a critical point of dysregulation in INS.

B cells in INS are transcriptionally poised for activation and plasmablast differentiation.

The expansion of activated B cells in INS prompted us to ask whether the transcriptional profiles of these cells reflect a state of hyperactivation, hypothesizing that B cells from affected children are intrinsically prone to activation, ultimately representing a potential defect in self-tolerance. Differential gene expression analysis between B cells from children with INS and controls identified 710 differentially expressed genes, of which 185 were upregulated in INS (**Figure 4F, Supplemental Data 2**). The transcriptional profile of B cells from the atopic disease

control more closely resembled that of INS than healthy controls, but its inclusion in our analysis allowed us to define a B cell transcriptional signature that is specific to INS. Genes enriched in INS B cells were strongly associated with type-I interferon responses, BCR signaling, and antibody production, all consistent with our previous findings (**Figure 4G**) (Al-Aubodah et al., 2023).

Independent differential gene expression analyses on naïve, activated, and memory B cells uncovered significant overlap in differentially expressed genes between these populations (**Figure 4H, Supplemental Data 3**). Pathway analysis showed that even naïve B cells from children with INS preferentially expressed genes involved in B cell activation, suggesting a transcriptional poise for activation even prior to antigen encounter (**Supplemental Figure 4D**). Core components of BCR signaling like *CD19*, *CD79B*, and downstream mediators such as *BANK1* and *BLNK* were preferentially expressed by naïve and activated B cell in INS (**Figure 4I**). These cells also expressed elevated levels of transcription factors that orchestrate B cell activation and differentiation, including *SPI1*, *SPIB*, *POU2F2*, and *POU2AF1* (**Figure 4I**) (Laidlaw and Cyster, 2021). In line with increased BCR signaling, *NR4A1* (Nur77), a sensitive marker of BCR engagement, was preferentially expressed across naïve, activated and memory B cells in INS (**Figure 4I**) (Mueller et al., 2015). Upregulation of *CD48* and *CD53*, molecules involved in the formation of the immunological synapse, further supports the presence of a hyperactivated B cell phenotype (**Figure 4I**). Interrogation of transcription factor regulons using the CollecTRI gene regulatory network resource confirmed that activated B cells in INS were enriched for transcription factor programs associated with lymphocyte activation, proliferation, and survival (**Figure 4J, Supplemental Figure 4E**) (Müller-Dott et al., 2023).

Consistent with the increased propensity for extrafollicular responses, expression of the EBI2 gene *GPR183*, a homing receptor that retains B cells in extrafollicular niches, was elevated in INS (**Figure 4I**) (Gatto and Brink, 2013). Likewise, expression of *TNFRSF13B*, encoding the APRIL/BAFF receptor TACI that is critical for extrafollicular responses, were elevated in memory B cells in INS (**Figure 4I**) (Elsner and Shlomchik, 2020). As extrafollicular responses are associated with the emergence of T-bet^{+} B cells, we assessed T-bet expression in INS B cells. As expected, the expression of the T-bet gene *TBX21* was most frequent in atBCs (B8) and did not differ between INS and controls (**Figure 4K**). However, actMBCs (B7) in INS showed significantly higher of frequencies of *TBX21*-expressing cells, suggesting enhanced extrafollicular skewing during B cell activation.

Finally, to determine whether this hyperactivated state translated into greater antibody responses, we isolated B cells from children with INS and healthy controls and stimulated them *in vitro* to induce plasmablast differentiation. Indeed, B cells from children with INS showed a markedly higher propensity to convert into plasmablasts relative to healthy controls (**Figure 4L**). Collectively, these data demonstrate that B cells in INS are prone to hyperactivation and more readily develop into antibody-secreting cells underscoring a major defect in B cell tolerance mechanisms.

The B cell repertoire in INS is enriched with V_H4-39 BCRs.

Defective B cell tolerance can result in the development of an aberrant or skewed B cell repertoire, often with an increased presence of autoreactive B cells, as clones that should remain tolerized or be deleted gain functional competence and ultimately contribute to the mature B cell pool (Bashford-Rogers et al., 2019; Deguine and Xavier, 2024). The nature of the B cell

repertoire in INS is unknown. Assessment of BCR isotypes in INS showed decreased use of *IGHD* BCRs and a concomitant increase in *IGHM* BCRs amongst naïve (B0, B1, B9) and naïve-act (B3) B cells (**Figure 5A, Supplemental Figure 5A**). This decrease in *IGHD* was also apparent in actMBC and MZ-like B cells and was similarly observed in the disease control (**Figure 5A**). Beyond isotype usage, INS B cells were significantly enriched for BCRs using *IGHV4-39* and *IGHV4-59* heavy chains, both of which were previously associated with autoreactivity in systemic lupus erythematosus, anti-phospholipid syndrome, multiple sclerosis, and rheumatoid arthritis (**Supplemental Figure 5B**) (Bashford-Rogers et al., 2019; Dieudonné et al., 2024; von Büdingen et al., 2012). Of the two, only *IGHV4-39* (V_H4-39) was significantly enriched across naïve, activated, and memory compartments, and even persisted into the plasmablast pool, denoting a selection or survival advantage for these $V_H4\text{-}39^+$ BCRs in INS as has been recently suggested in other autoimmune settings (**Figure 5B, C**) (Dieudonné et al., 2024). While the overall cellular composition of $V_H4\text{-}39^+$ B cells was similar between INS and controls, comparisons of B cell composition within the complete repertoire to the $V_H4\text{-}39^+$ repertoire showed that $V_H4\text{-}39^+$ BCRs were censored from entering the plasmablast pool within control children, whereas this censoring was not observed in INS (**Figure 5D**). Within the $V_H4\text{-}39^+$ pool, IgD usage was markedly reduced in INS mirroring what was observed in the complete repertoire (**Figure 5E**). Accordingly, $V_H4\text{-}39^+$ B cells were more retained within the IgD^+ compartment in control children than in children with INS, again highlighting the absence of censoring of $V_H4\text{-}39^+$ B cells from the post-antigenic B cell compartment in INS (**Figure 5E**).

We then sought to determine whether there were differences in clonality between INS and control. B cell clonality was comparable between INS and controls, with six of the eight children with INS showing high clonal expansion (defined as ≥5 B cells/clone) and two of the four

controls (**Supplemental Figure 5C, D**). Nevertheless, both atBCs and actMBCs were enriched in the expanded B cell pool of children with INS, supporting the preferential activation of B cells through the extrafollicular route (**Supplemental Figure 5E**). Isotype usage was not significantly different between clonally expanded B cells in INS and controls (**Supplemental Figure 5F**). Importantly, consistent with increased *IGHV4-39* usage in INS, $V_H4\text{-}39^+$ B cells were present in the clonally expanded repertoire in seven of the eight children with INS and in two controls, with the highest abundance in four of the children with INS (**Figure 6F, G**). Together, these findings reveal a skewed B cell repertoire in children with INS that favours $V_H4\text{-}39^+$ B cells, thereby underlining the presence of a defect in B cell tolerance.

DISCUSSION

The recent discovery of autoantibodies in idiopathic podocytopathies suggests that these diseases have a shared autoimmune basis. However, the immune mechanisms that lead to the production of anti-slit diaphragm autoantibodies remain unknown. In this study, we identify CRB2 as a slit diaphragm antigen that is frequently targeted by autoantibodies in idiopathic podocytopathies. Anti-CRB2 autoantibodies are more prevalent in adults with MCD and primary FSGS than in children with INS, and they can occur alongside anti-Nephrin autoantibodies, possibly via epitope spreading. In children, anti-slit diaphragm autoantibodies correlate with frequencies of T-bet^{+} CD21^{low} atBCs, suggesting a link between extrafollicular responses and podocyte-directed autoimmunity. While atBCs are similarly expanded in adults, we find no correlation with the abundance of anti-slit diaphragm autoantibodies. Instead, a more extensive B cell defect is evident in adults. We also demonstrate that B cell activation in children with INS is dysregulated and associated with a B cell repertoire enriched with V_H4-39^{+} clonotypes. Ultimately, our study suggests that podocyte-reactivity originates from a broadly dysregulated B cell landscape, likely through the extrafollicular activation of podocyte-reactive B cell clones.

The discovery of anti-CRB2 autoantibodies in this study adds to the growing list of anti-slit diaphragm autoantibodies prevalent in idiopathic podocytopathies, alongside anti-Nephrin, anti-NEPH1, and anti-Podocin (Hengel et al., 2024; Raglianti et al., 2025; Watts et al., 2022). Of these, only anti-Nephrin and anti-CRB2 have already been shown to be pathogenic in mouse models, causing cytoskeletal derangements in podocytes (Hada et al., 2022; Hengel et al., 2024). In this study, we were better able to detect anti-CRB2 autoantibodies than anti-Nephrin, resulting in a higher seroprevalence for anti-CRB2. Standardized quantitative detection methodologies are needed to make reliable comparisons between distinct anti-slit diaphragm autoantibodies in

various cohorts of idiopathic podocytopathies. Notably, seropositivity for both anti-CRB2 and anti-Nephrin exhibited significant variability over time in any given individual, potentially reflecting fluctuations in the podocyte-specific B cell response due to immunosuppressive treatment or disease progression. Consequently, we are likely underestimating the prevalence of Nephrin/CRB2-directed autoimmunity within this cohort. This is consistent with a recent study showing that up to 90% of children with INS carry anti-Nephrin autoantibodies during active disease in the absence of previous immunosuppression, with much lower seroprevalence observed in relapses following exposure to immunosuppressive treatment (Hengel et al., 2024).

While anti-Nephrin was similarly present in children and adults with idiopathic podocytopathies, anti-CRB2 autoantibodies were significantly more prevalent and abundant in adults than children. This suggests that the accumulation of anti-CRB2 autoantibodies may depend on a more sustained podocyte-reactive B cell response. Indeed, isotype-switched (IgG/IgA) anti-CRB2 autoantibodies were much more common in adults than unswitched (IgM) versions, possibly reflecting a greater degree of class-switching. Similarly, adults were more likely to be seropositive for both anti-CRB2 and anti-Nephrin autoantibodies than children (25.8% vs. 11.8%), suggesting that idiopathic podocytopathy in adults is associated with a greater degree of B cell dysregulation. Using a mouse model, we showed that epitope spreading may contribute to the emergence of these autoantibodies. This process, which can often take years to progress, is a well-established feature of autoimmune diseases and can correlate with clinical severity, as is the case in systemic lupus erythematosus where epitope spreading drives the diversification of autoantibodies targeting ribonucleoprotein complexes (Suurmond and Diamond, 2015; Vanderlugt and Miller, 2002). Notably, MCD and FSGS can also occur secondary to systemic lupus erythematosus, further linking epitope spreading to the pathogenesis

of podocytopathy (Hertig et al., 2002; Hu et al., 2016). While our findings suggest a potential role for epitope spreading in the breach of tolerance to slit diaphragm antigens, definitive proof is still lacking. To this end, longitudinal studies tracking the evolution of the podocyte-directed autoantibody response from disease onset are critical for addressing the role of epitope spreading in the generation of anti-slit diaphragm autoantibodies, as well as the utility of these autoantibodies as clinical biomarkers.

We previously demonstrated that T-bet^{+} CD21^{low} atBCs were expanded in children with INS (Al-Aubodah et al., 2023). Here, we extend this observation to adult MCD and primary FSGS, supporting a shared autoimmune origin for idiopathic podocytopathies. These B cells are frequently expanded in systemic autoimmunity harbouring a pool of autoreactive clones, giving rise to short-lived plasmablasts through extrafollicular responses (Claes et al., 2016; Holla et al., 2021; Sutton et al., 2021). Consequently, atBCs correlate with titers of pathogenic autoantibodies in autoimmune diseases like systemic lupus erythematosus (Jenks et al., 2018). Furthermore, recent work in mice showed that extrafollicular B cells may be involved in expanding autoantibody responses through epitope spreading (Fahlquist-Hagert et al., 2023). Notably, we demonstrate that atBCs and isotype-switched plasmablasts correlate with anti-Nephrin and anti-CRB2 titers in children with INS, particularly when both autoantibodies are considered together, thereby positioning extrafollicular responses as the possible origin for anti-slit diaphragm autoantibodies. Nevertheless, concrete proof will require tracking CRB2/Nephrin-specific B cell clones using tetramers or antibody cloning approaches.

Unlike children with INS, the expanded atBCs did not correlate with autoantibody titers in adults with MCD and FSGS. The concomitant expansion of cMBCs in adults suggests a greater degree of B cell dysregulation than in children, spreading to involve germinal center

responses in secondary lymphoid organs where cMBCs mature their BCRs. Evidence suggests that autoreactive germinal center responses may be seeded by atBCs themselves (Gao et al., 2024). The long-lived plasma cells generated in germinal centers mainly reside in the bone marrow, are less responsive to steroid therapy than short-lived plasmablasts arising from extrafollicular responses and have undergone significant antibody maturation (Mumtaz et al., 2012). Consequently, the mobilization of podocyte-reactive B cells into germinal centers – as well as the consequential development of high affinity autoantibodies – could underlie the increased propensity for steroid resistance and disease severity in adults with idiopathic podocytopathies (Al-Aubodah et al., 2025). This could also explain the lack of correlation between circulating B cell subsets and autoantibody titers in adults and the increased rate for isotype-switching observed for anti-CRB2 autoantibody in adults observed in this study.

Considering the immune landscape in children with INS as being more proximal to the initial breach in tolerance, we employed single-cell RNA-sequencing to investigate the mechanisms that drive the recruitment of podocyte-reactive B cells into the post-antigenic B cell compartment. While the findings in this study are consistent with our previous report using single-cell RNA-sequencing to profile PBMC from children with INS, the dataset presented here contains many more B cells (93,766 vs. 5,210 B cells) and donors (eight vs. four children with INS) while also linking gene expression data with BCR sequences. This allowed us to pinpoint the defect to B cell activation, with both naïve and memory B cells in children with INS showing greater transcriptional poise for activation. B cell activation in INS is skewed towards the extrafollicular route as reflected by the accumulation of atBCs and MZ-like B cells, and increased expression of key extrafollicular response genes within activated subsets, including *GPR183* (EBI2), *TNFRSF13B* (TACI), and *TBX21* (T-bet). Furthermore, the decreased

prevalence of IgD BCRs among activated B cells in children with INS suggests a defect in peripheral tolerance, as the retention of IgD BCRs is linked to the induction of anergy following aberrant B cell activation (Duty et al., 2008; Sabouri et al., 2016). This dysregulated B cell activation in INS would recruit a wide range of antigen specificities into the post-antigenic compartment, which may include podocyte-specific B cell clones that can mediate podocyte-directed autoimmunity. The mechanisms underlying this defective tolerance are likely polygenic, with genetic variants affecting BCR signaling (e.g. *PLCG2*) and peripheral tolerance (e.g. MHC-II polymorphisms) that have previously been associated with INS contributing to this phenotype (Barry et al., 2023; Debiec et al., 2018; Downie et al., 2023; Dufek et al., 2019; Gbadegesin et al., 2015).

Consistent with impaired tolerance, we observed a skewed BCR repertoire in INS that is enriched with clones bearing V_H4-39 BCRs. While the general autoreactive potential of V_H4-39 BCRs remains unclear, they are frequently associated with autoantibodies in systemic lupus erythematosus, anti-phospholipid syndrome, and multiple sclerosis (Bashford-Rogers et al., 2019; Dieudonné et al., 2024; von Büdingen et al., 2012). Similarly, other V_H4 BCRs, like V_H4-34 and V_H4-59, have been repeatedly associated with autoreactivity in autoimmune settings (Bashford-Rogers et al., 2019; Richardson et al., 2013). While investigations of the B cell repertoire in podocytopathies remain limited, data in a recent report also showed increased usage of V_H4-39 by B cells from children with INS (Ye et al., 2023). A similar observation was made in adults with membranous nephropathy, indicating a possible link between V_H4-39 and podocyte-reactivity (Su et al., 2021). It has recently been shown that V_H4-39$^+$ B cell clones appear to be censored from the antibody-secreting cell pool in healthy individuals, but progress into plasma cells in people with anti-phospholipid syndrome (Dieudonné et al., 2024). Similarly, we

demonstrate that $V_H4\text{-}39^+$ B cell clones were prevalent in the plasmablast pool in children with INS but were excluded from this pool in healthy individuals. As checkpoints within germinal centers may limit the entry of autoreactive B cells into the antibody-secreting cell compartment, extrafollicular responses may represent an alternative route for autoreactive B cells, thus leading to the accumulation of $V_H4\text{-}39^+$ plasmablasts in INS (He and Vinuesa, 2024; Pugh-Bernard et al., 2001; Richardson et al., 2013). This would be analogous to the inherently autoreactive $V_H4\text{-}34^+$ B cell clones seen in systemic lupus erythematosus and other systemic autoimmune diseases (Pugh-Bernard et al., 2001). Moreover, $V_H4\text{-}39$ antibodies have also been associated with polyreactivity, particularly in the case of chronic lymphocytic leukemia, and may therefore be involved in epitope spreading (Gounari et al., 2012). However, it remains to be determined whether the $V_H4\text{-}39^+$ B cells identified in this study include podocyte-reactive clones that may contribute to the podocyte-directed autoimmune response.

In summary, we identify anti-CRB2 as a new anti-slit diaphragm autoantibody that is prevalent in idiopathic podocytopathies, and we propose epitope spreading as a possible mechanism for their emergence. We demonstrate a link between autoantibody production and extrafollicular B cell responses in children with INS, while highlighting a greater degree of B cell dysregulation involving follicular responses in adults with MCD and primary FSGS. Our work provides a much-needed immune-based rationale for understanding the immunopathogenic mechanisms underlying the idiopathic podocytopathy disease spectrum, emphasizing the importance of developing antibody and cellular biomarkers for disease prognostication and informing effective treatment strategies.

MATERIALS AND METHODS

Patient cohort

Blood from 104 patients with glomerulopathies and 48 healthy controls were collected and used in this study (Supplemental Table 1). Of these, 75 patients and 44 healthy controls were enrolled in the McGill University Health Centre Kidney Disease Biorepository (MUHC-14-466, T.T.), while 29 patients and 4 healthy controls were enrolled in the CHILDNEPH study biobank (CHREB-16-2186, S.S.) (Al-Aubodah et al., 2023; Samuel et al., 2014). In total, there were 55 children enrolled in the study, 19 of whom were non-biopsied and classified as having SSNS (*N*=18) or SRNS (*N*=1) while the remaining were diagnosed through biopsy with MCD (*N*=24), primary FSGS (*N*=8), membranous nephropathy (*N*=2), or other glomerulopathies (*N*=2) (**Supplemental Table 1**). All 49 adults had biopsy-proven disease, including MCD (*N*=10), FSGS (*N*=21), membranous nephropathy (*N*=6), and other glomerulopathies (*N*=12) (**Supplemental Table 1**).

Children were considered in active disease when proteinuria at time of blood draw exceeded 0.25 g/mmol on the urinary dipstick or 1 g/day with other measurements, and a diagnosis of either first episode or relapse was made by a nephrologist in a contemporary clinical evaluation. Adults were considered in active disease when proteinuria at time of blood draw exceeded 1 g/day and a diagnosis of either first episode or relapse was made by a nephrologist in a contemporary clinical evaluation. For children, remission was defined by a negative or trace urinary dipstick measurement or proteinuria less than 200 mg/day, while for adults it was defined by a proteinuria of less than 300 mg/day (KDIGO, 2021). For children, steroid resistance was defined by a persistent proteinuria of >200 mg/day despite four weeks of daily steroid therapy (equivalent of prednisone at 60 mg/m^2/day) and a two week confirmation period with escalated

steroid treatment, while in adults it was defined by a persistent proteinuria of >3500 mg/day with a reduction of <50% from baseline with 16 weeks of steroid therapy (equivalent of prednisone at 1 mg/kg/day) (KDIGO, 2021; Trautmann et al., 2020). Healthy controls were defined as patients without a diagnosis of kidney, autoimmune, allergic, hematologic or neoplastic disease. Serum samples were obtained from all participants and 28 of the healthy controls, while PBMC were available for 43 patients and 35 healthy controls (Supplemental Table 1).

Clinical data was collected retrospectively when available for each patient followed at the McGill University Health Centre using their electronic medical file. For patients enrolled in the CHILDNEPH cohort, limited clinical data was available through the CHILDNEPH registry. All participants and/or their legal guardians gave written informed consent to be enrolled in the study, and biospecimen were used in accordance with our stand operating protocol (MUHC-15-341, T.T.). Research ethics board approvals were obtained for all centres involved in this study.

Mice

Wildtype C3H/HeN (Charles River Laboratories) were bred at the Research Institute of the McGill University Health Centre. All mice were raised in specific pathogen-free conditions, and male 8-week-old mice were used in this study. Experiments were performed according to the Canadian Council on Animal Care and to institutional guidelines at McGill University, and ethical guidelines approved by local committees at the RI-MUHC.

Human anti-CRB2 and anti-Nephrin ELISAs

Wells of ELISA plates (Nunc-Immuno Plate, MaxiSorp, 96-well, ThermoFisher) were coated overnight at 4°C with 1.00 µg of $CRB2_{597-943}$ or 0.13 µg of Nephrin in 0.2 M sodium

carbonate-bicarbonate solution. Antigens were the extracellular domain of human CRB2 (E597-V943) produced in *E. coli* or full-length human Nephrin (SinoBiological) produced in HEK293 cells (Hamano et al., 2018). After overnight coating, plates were washed three times with washing solution (PBS+0.2% Tween) before blocking with blocking solution (PBS+2% BSA and 0.2% Tween) for 1 hour. Then, plates were loaded with 100 µL of standards and serum samples in duplicates. The standard curve was generated using seven serial dilutions of polyclonal rabbit anti-human CRB2 antibody (custom produced by MediMabs, Montreal, using human $CRB2_{597-943}$ recombinant protein) or monoclonal sheep anti-human Nephrin antibody (RnD systems). Sera was diluted 1:1000 (anti-CRB2) or 1:500 (anti-Nephrin) in blocking buffer. After 2 hours of incubation, plates were washed three times and incubated for 1 hour with anti-rabbit IgG-HRP (anti-CRB2) or anti-goat IgG-HRP (anti-Nephrin) antibodies (Abcam) for the standard curve, and anti-human IgG-HRP antibodies (Abcam) for sera. Plates were then incubated with 100 µL of 3,3',5,5'-tetramethylbenzidine substrate solution (Bethyl laboratories) for 1 minute (anti-CRB2) or 5 minutes (anti-Nephrin) before the reaction was stopped with 2 M H_2SO_4 (Sigma-Aldrich). The results were read with a TECAN plate reader at an absorbance of 450 nm and titers were calculated using a four-parameter logistic curve. Uncoated plates loaded with the same serum dilutions were run to detect background. As the background was <1% of detected optical density, it was ignored. Positivity cut-offs were determined as $Cutoff = x\square + SD \times f$, where $x\square$ is the mean titer the healthy control population (presumed seronegative) and SD is the standard deviation. The multiplier f is calculated as $f = t_{1-0.05} + (1/N)$, where $t_{1-0.05}$ is the critical t-value for an α-value of 0.05 and N is the size of the cohort.

Confocal imaging of human flash frozen kidneys

Flash frozen kidney biopsies from seven patients were prepared by the McGill University Health Centre kidney pathology department. Kidneys were sectioned at 4 µm, air dried for 30 minutes, and subjected to treatment with 95% ethanol for 10 minutes at -20°C. Sections were then washed three times in PBS before fixing with 4% paraformaldehyde (ThermoFisher) for 15 minutes. After another three washes in PBS, blocking was performed with PBS containing 3% bovine serum albumin (Sigma-Aldrich) and 2% FBS (Wisent) for 1 hour. Staining with rabbit anti-CRB2 (1:100, Sigma-Aldrich), guinea pig anti-Nephrin (1:100, Progen), and mouse anti-human IgG (1:750, Abcam) was carried overnight at 4°C. Sections were washed again in PBS, and stained with anti-rabbit AlexaFluor 488 (1:1000, Cell Signaling) and anti-mouse AlexaFluor 555 (1:1000, Cell Signaling) for 1 hour at room temperature. Staining with DAPI (1:1000, ThermoFisher) was carried out afterwards for 15 minutes, and the sections were mounted with Aquamount (Fisher Scientific). Immunofluorescence images were captured with a Zeiss LSM780 confocal microscope using a 20X objective. High-resolution structured illumination microscopy images were captured using a Zeiss LSM880 SIM confocal microscope. Laser intensity was kept the same for all images across a single experiment. Images were processed and quantified using Zeiss Microscopy Software v3.12 (Carl Zeiss AG).

Mouse model for autoimmune podocytopathy

Recombinant mouse $Crb2_{601-940}$ or $Nephrin_{384-731}$ produced in *E.coli* in PBS (1 mg/mL) was emulsified 1:1 with Complete Freund's Adjuvant (Millipore Sigma), and 100 µL was injected bilaterally at the base of tail for a total dose of 100 µg (Hada et al., 2022). Mice were re-challenged after 2 and 4 weeks with 100 µg of antigen emulsified in Incomplete Freund's

Adjuvant (Millipore Sigma) injected subcutaneously at both flanks. Urine was collected manually at the indicated time points, and urinary albumin (Bethyl Laboratories) and creatinine (Cayman Chemical) concentrations were measured by ELISAs according to manufacturer instructions. The former was normalized to the latter to obtain urinary albumin-to-creatinine ratios. Serum was collected from saphenous veins.

Mouse anti-Crb2 and anti-Nephrin ELISAs

ELISAs for anti-Crb2 and anti-Nephrin in mice were conducted as described for human ELISAs. Coating antigens were replaced for $mCrb2_{601-940}$ or $mNephrin_{384-731}$. Serum samples were diluted 1:1000, 1:5000, or 1:25000 to ensure that optical densities fall within the linear range of the ELISAs. Detection was carried out using anti-mouse IgG-HRP antibodies diluted 1:1000 in blocking buffer (Abcam).

B cell profiling by flow cytometry

Cryopreserved PBMC were thawed in warm RPMI 1640 media (Wisent) completed with 10% FBS (Wisent), 10,000 U/ml penicillin-streptomycin (Gibco), 1% MEM nonessential amino acids (Wisent), 1% 1M HEPES solution (Wisent), and 1% 100 mM sodium pyruvate. Cells were rested at 37°C for 2 h in a 5% CO_2 incubator before staining. A viability of over 90% was confirmed by Trypan blue, and a maximum of 1×10^6 cells were transferred into a 96-well v-bottom plate for staining per flow cytometry panel. Cells were washed once in ice-cold PBS supplemented with 2% FBS and labelled with the Fixable Viability eFluor 780 dye (1:1000, ThermoFisher Scientific). After a 15-minute incubation at 4°C, cells were washed again in PBS+2% FBS, and incubated with Fc receptor block (1:50, BD Biosciences) for 15 minutes.

Cells were washed and staining for extracellular markers was performed using antibody cocktails prepared in ice-cold PBS+2% FBS and Brilliant Stain Buffer (1:2, BD Biosciences): anti-human CD3ε BV785 (1:50, OKT3, BioLegend), anti-human CD19 BV605 (1:20, SJ25C1, BD Biosciences), anti-human CD20 AlexaFluor 700 (1:50, 2H7, BioLegend), anti-human CD21 BV421 (1:20, B-ly4, BD Biosciences), anti-human CD27 PE-Cy7 (1:20, M-T271, BD Biosciences), anti-human CD10 BUV737 (1:20 HI10a, BD Biosciences), anti-human CD38 BUV737 (1:20, HB7, BD Biosciences), anti-human CD11c PerCp-Cy5.5 (1:20, B-ly6, BD Biosciences), anti-human IgD BV510 (1:20, IA6-2, BioLegend), anti-human IgM AlexaFluor 488 (1:40, MHM-488, BioLegend), anti-human FcRL5 APC (1:20, 509f6, BioLegend), anti-human CD24 PE (1:20, ML5, BD Biosciences), anti-human CD1c BV711 (1:20, L161, BioLegend), anti-human CXCR5 APC (1:20, J252D4, BioLegend), anti-human TACI PE (1:20, 1A1, BioLegend), anti-human GPR183 PerCp-Cy5.5 (1:50, SA313E4, BioLegend), and anti-human CD23 APC (1:20, EBVCS-5, BioLegend). Cells were incubated at 4°C for 20 minutes, washed, and then fixed/permeabilized using the eBioscience Foxp3/Transcription Factor Staining Buffer Set (eBioscience). Cells were then washed with 1X permeabilization buffer (eBioscience) and stained for intracellular markers using antibody cocktails prepared in the same buffer: anti-Ki-67 BUV395 (1:50, B56, BD Biosciences), and anti-T-bet PE (1:20, 4B10, BioLegend). Two final washes were performed in permeabilization buffer and PBS+2% FBS before cells were acquired on the BD LSR Fortessa X-20. Data were analyzed using FlowJo v10.8 software (FlowJo, LLC).

Single-cell RNA-sequencing: library preparation and sequencing

Cryopreserved PBMC were thawed as described in the previous section. Cells were washed with ice-cold PBS+2% FBS and labelled with an antibody cocktail containing Fixable Viability eFluor 780 dye (ThermoFisher Scientific, 1:1000), anti-human CD19 BV605 (1:20, SJ25C1, BD Biosciences), anti-human CD3ε BV785 (1:50, OKT3, BioLegend), AlexaFluor 700 anti-human CD20 (1:50, 2H7, BioLegend) and anti-human CD10 BUV737 (1:20, HI10, BD Biosciences) prepared in PBS+2% FBS at 4°C for 15 minutes. After washing, cells were filtered through 70 μm mesh and total live mature B cells (Viability eFluor 780^{-} $CD19^{+}$ $CD10^{low}$ $CD3\varepsilon^{-}$) were isolated via fluorescence-activated cell sorting using the BD FACSAria Fusion with >99% purity. B cells were washed in PBS+0.04% bovine serum albumin, concentrated to 1,500 cells/μL, and processed using the Chromium Next GEM Single Cell 5' v2 (PN-1000263) and Chromium Single Cell Human BCR Amplification (PN-1000253) kits in three batches (*N*=4 samples/batch) targeting 10,000 to 15,000 captured cells. Complementary DNA was synthesized and Chromium Single Cell 5' gene expression and V(D)J libraries were prepared according to manufacturer instructions. Libraries were sequenced on a NovaSeq6000 (Illumina) to a median sequencing depth of 30,000 reads/cell for gene expression libraries and 5,000 reads/cell for V(D)J libraries.

Single-cell RNA-sequencing: preprocessing and quality control of gene expression data

FASTQ reads were aligned to the GRCh38 reference genome v1.2.0 (refdata-cellranger-GRCh38-1.2.0) and count matrices were generated using CellRanger v7.1.0. All preprocessing and quality control steps were performed using the Seurat v5.0.0 R package (Hao et al., 2021). Briefly, contaminating non-B cells expressing *CD3G*, *CD14*, *LILRA4* or hemoglobin genes were removed, and cells with <200 of >2700 features, >8% transcripts belonging to mitochondrial

genes, or <14% transcripts corresponding to ribosomal protein genes were filtered out as doublets or nonviable cells. Mitochondrial genes, ribosomal genes, *MALAT1* and *XIST* were regressed from the dataset to prevent their impact on downstream clustering.

Single-cell RNA-sequencing: generating and annotating clusters

The reciprocal principal component analysis (PCA) method in Seurat v5.0.0 was used to generate B cell clusters that were uniformly present across individuals and batches. Expression data were normalized, and variable features were identified for each independent sample. Features that were consistently variable across samples were then selected (SelectIntegrationFeatures), scaled, and used to perform an initial PCA. The resulting principal components (PCs) were used to identify integration anchors (FindIntegrationAnchors) and integrate the data (IntegrateData). The integrated data was scaled and PCA was performed again. A uniform manifold approximation and projection (UMAP) was generated on *k*NN values calculated with 10 PCs, and Louvain clusters were generated at a resolution of 0.5. A single cluster of cells corresponding with contaminating natural killer cell were removed and a new UMAP was generated using 9 PCs and a resolution of 0.5.

Marker sets for each cluster were generated by running differential gene expression analysis between the query cluster and all other B cells using the FindAllMarkers function in Seurat v5.0.0 (Supplemental Figure 2B). The resulting gene lists were filtered to only include genes expressed in at least 10% of cells and were subsequently used to assign cluster identities (Figure 4A). Broadly, naïve B cells were identified based on the expression of *BACH2*, *TCL1A*, *FCER2*, and *IL4R*; activated B cells (Act) using *CD69*, *FOS*, and *FOSB*; memory B cells (MBC) using *BCL2A1*, *IGHA1*, and *CD27*; and plasmablasts (PB) using *PRDM1*, and *JCHAIN*.

Single-cell RNA-sequencing: differential abundance testing

Overlapping cellular neighbourhoods reflective of distinct cell states were generated on the integrated UMAP embeddings using MiloR v1.10.0 (Dann et al., 2022). Here, a *k*NN graph was built using the buildGraph and makeNhoods function on randomly selected cells in the data set (5% of total), 8 PCs, and $k = 50$. These parameters were fine-tuned through manual inspection of neighbourhood sizes as was recommended through the standard MiloR workflow. Shifts in proportions of distinct neighbourhoods between children with INS and controls was tested using the testNhoods function with a spatial *FDR* adjusting for the overlap between neighbourhoods of < 0.1 considered as significant.

Single cell RNA-sequencing: differential gene expression and transcription factor regulons

To identify a robust set of genes that are differentially expressed, pseudobulk differential gene expression analysis was carried out using Muscat v1.13.1 (Crowell et al., 2020). Pseudobulk data were generated by aggregating normalized and log-transformed gene counts at the sample and cell cluster levels using the aggregateData function. Differential gene expression was then performed using edgeR and differentially expressed genes were considered as those with a $|\log_2(\text{fold change})| < 0.65$, $P_{adj} < 0.05$, and were expressed in at least 10% of cells. Gene set enrichment analysis (GSEA) was performed on unfiltered gene lists ordered by $\log_2$(fold change) using the GSEA App (Broad Institute). Pathway analysis was performed using g:Profiler. For both GSEA and pathway analyses, the Gene Ontology and Reactome databases were used including gene sets that contained at least 5 and no more than 500 genes. Scores for transcription factor regulons, obtained from the CollecTRI gene regulatory network, were inferred for every

cell using decoupleR v2.9.7 (Müller-Dott et al., 2023). Scaled scores were used for comparisons of regulons between children with INS and controls.

Single-cell RNA-sequencing: V(D)J processing and gene annotation

Demultiplexed pair-end FASTQ reads were processed via CellRanger v7.1.0 and aligned to the GRCh38 human reference genome (refdata-cellranger-vdj-GRCh38-alts-ensembl-5.0.0). The resulting outputs were then processed using the Immcantation pipeline. The initial germline annotations were performed using IgBLAST v1.22.0 with the IMGT/V-Quest reference, and the outputs were converted to the adaptive immune receptor repertoire (AIRR) format using MakeDb.py from Change-O v1.3.0 (Giudicelli et al., 2005; Gupta et al., 2015; Ye et al., 2013). Only sequences with productive rearrangement and a CDR3 nucleotide sequence length that is a multiple of three were retained, and cells with no or multiple heavy chains were removed. If a cell had multiple light chains, the most abundant transcript was kept (or the first transcript listed in case of a tie). Finally, only cells present in the gene expression dataset following processing, quality control, and clustering steps were retained in the V(D)J data.

Single-cell RNA-sequencing: clonal lineage inference

Clonal lineages were inferred for each donor on productive heavy chain sequences with hierarchical clustering using SCOPer v1.3.0 (Gupta et al., 2017; Nouri and Kleinstein, 2018; Zhou and Kleinstein, 2019). Heavy chains with equivalent V and J genotypes and CDR3 lengths were parsed into partitions, and CDR3 nucleotide sequences within a 0.15 normalized Hamming distance from each other within each partition were defined as clones. Full-length consensus

germline sequences were reconstructed for each clone from the IMGT/V-Quest reference using Dowser v2.1.0 (Hoehn et al., 2022). Clone networks were then generated using the Dandelion v0.3.5 python package on the inferred clones and visualized through Scanpy v1.9.8 (Bashford-Rogers et al., 2013; Suo et al., 2024).

Single-cell RNA-sequencing: somatic hypermutation and class-switch recombination

Somatic hypermutation was calculated as the frequency of nucleotide mismatches from the germline sequence of the CDR1, CDR2, FWR1, FWR2, and FWR3 segments of the variable heavy chain using SHazaM v1.2.0 (Gupta et al., 2015). CSR was calculated as the frequency of cells with a constant heavy chain genotype that was not *IGHM* nor *IGHD*. The constant heavy chain genotype was obtained from the 'c_call' column of the CellRanger output.

B cell culture

Cryopreserved PBMC were thawed as described in the flow cytometry section. Cells were washed with ice-cold PBS+2% FBS and labelled with an antibody cocktail containing the Fixable Viability eFluor 780 dye (ThermoFisher Scientific, 1:1000), anti-human CD19 BV605 (1:20, SJ25C1, BD Biosciences), anti-human CD3ε BV785 (1:50, OKT3, BioLegend), and AlexaFluor 700 anti-human CD20 (1:50, 2H7, BioLegend). After a subsequent wash, cells were resuspended in ice-cold PBS+2% FBS, filtered through 70 μm mesh, and live B cells (Viability eFluor 780^{-} $CD19^{+}$ $CD20^{+}$ $CD3\varepsilon^{-}$) were isolated via fluorescence-activated cell sorting using the BD FACSAria Fusion with >99% purity. Cells were washed with and brought up in complete RPMI 1640 medium. Duplicate 40,000 cells were plated in 96-well round-bottom plates and stimulated with recombinant human CD40L-Ig (1 μg/mL, Invivogen), F(ab')2 goat anti-human

IgM/IgG (100 ng/mL, ThermoFisher), IL-21 (50 ng/mL, BioLegend), and IL-4 (10 ng/mL, BioLegend). After 4-day culture, cells were harvested and stained for flow cytometric evaluation of plasmablast ($CD27^{+}$ $CD38^{high}$) differentiation.

Statistical analysis

Statistical analyses were performed on R v4.4.0 or GraphPad Prism v10.2.2 software. Continuous variables are presented as median with 95% confidence intervals with each point representing a single individual, while categorical variables are presented as number of patients (percentage). *P*-values for differences in categorical variables were determined using a Fisher's exact test. Two-sided analyses between two unpaired groups were completed using Mann-Whitney U-tests, while paired groups were analyzed using Wilcoxon signed-rank tests. Comparisons between more than two groups were performed using Kruskal-Wallis tests and corrected with Dunn's post-hoc testing, or on-way ANOVA corrected with Tukey's post-hoc testing. Non-parametric Spearman correlations were used to obtain *r* and *P*-values when evaluating the relatedness of two parameters. For differential gene expression, gene set enrichment analysis, and pathway analysis, P_{adj}-values were determined using Wilcoxon rank-sum tests with Benjamini-Hochberg corrections. *P*-values < 0.05 were considered significant. No sample size calculations were conducted *a priori*, and no samples were excluded from the study. Serum samples were available for some individuals without associated PBMC and *vice versa*.

Online Supplemental Materials

Fig. S1 shows longitudinal autoantibody seropositivity, IgM/IgA autoantibody seropositivity, autoantibody correlation with disease parameters, and representative IgG staining in kidney

biopsies and is associated with Fig. 1. Fig. S2 shows the flow cytometry gating strategy, the frequency of key B cell populations from total lymphocytes, and alternative definitions of atypical B cells and is associated with Fig. 2. Fig. S3 shows correlation between atypical B cells and plasmablasts with autoantibodies in adults and is associated with Fig. 3. Fig. S4 shows sample-level B cell distributions for the single-cell RNA-sequencing dataset, cluster markers, pathway analysis results, and CollecTRI results and is associated with Fig. 4. Fig. S5 shows additional plots linked with isotype and *IGHV* gene usage for the single cell RNA-sequencing dataset, and analyses associated with the clonally expanded B cell pool and is associated with Fig. 5. Table S1 provides detailed characteristics for patients involved in this study. Data S1 lists the differentially expressed genes for each B cell cluster against all other B cells. Data S2 lists the differentially expressed genes for total B cells in children with INS against controls. Data S3 lists the differentially expressed genes for each B cell metacluster (naïve, activated, memory) in children with INS against controls.

DATA AVAILABILITY

Raw sequencing data and processed count matrices were deposited in the NCBI Gene Expression Omnibus (GEO) under the accession number GSE307080. The results of all differential gene expression analyses and pathway analyses are included in the Supplemental Data files of this paper. Public data repositories used include the Gene Ontology and Reactome databases accessed by g:Profiler (https://biit.cs.ut.ee/gprofiler/gost) for pathway analyses and CollecTRI for transcription factor regulon assessment. The GRCh38 human reference genome was used for gene expression sequence alignment. The IMGT/V-Quest human reference was used for V(D)J sequence alignment.

ACKNOWLEDGEMENTS

We would like to thank all study participants, their families, researchers, physicians, and personnel involved in the McGill University Health Centre Kidney Disease Biorepository and the CHILDNEPH biobanks. We also thank I. Ragoussis, H. Djambazian, A. Harutunian, and Y. Wang at the McGill Genome Centre for their services through the 10X platform, and M-H. Lacombe, E. Iourtchenko, and H. Pagé-Veillette at the Research Institute of the McGill University Health Centre Immunophenotyping Core for access to flow cytometry equipment and cell sorting services.

This work was supported by a Canadian Institute of Health Research (CIHR) project grant (PJT-166006 to T.T., C.P, and S.S. and PJT-192017 to T.T. and C.P.) and a Kidney Foundation of Canada (KFoC) Kidney Health Research grant (24KHRG-1247769 to T.T. and C.P.). T.A. was supported by a Doctoral Award from CIHR and S.L. by a Krescent Post-Doctoral Fellowship from KFoC.

Author contributions: T. Al-Aubodah: conceptualization, data curation, formal analysis, investigation, methodology, software, validation, visualization, writing – original draft, writing – review & editing. S. Leclerc: conceptualization, data curation, formal analysis, investigation, methodology, validation, visualization, writing – original draft, writing – review & editing. L. Aoudjit: data curation, investigation, methodology. R. Samanta: resources. C. Mammen: resources. A. Dart: resources. A. Lapeyraque: resources. C. Morgan: resources. M.L. Downie: resources. S. Mori: resources. K. Yan: resources. S.M. Samuel: project administration, resources, writing – review & editing. C.A. Piccirillo: conceptualization, funding acquisition, project administration, resources, supervision, writing – original draft, writing – review & editing. T. Takano: conceptualization, funding acquisition, project administration, resources, supervision, writing – original draft, writing – review & editing.

SUPPLEMENTAL DATA

Supplemental Table 1 – detailed patient characteristics (.xlsx)

Supplemental Data 1 – lists of differentially expressed genes for each B cell cluster against all other clusters (.csv)

Supplemental Data 2 – list of differentially expressed genes for total B cells in INS against controls (.csv)

Supplemental Data 3 – lists of differentially expressed genes for each B cell metacluster in INS against controls (.xlsx)

FIGURES AND FIGURE LEGENDS

Figure 1

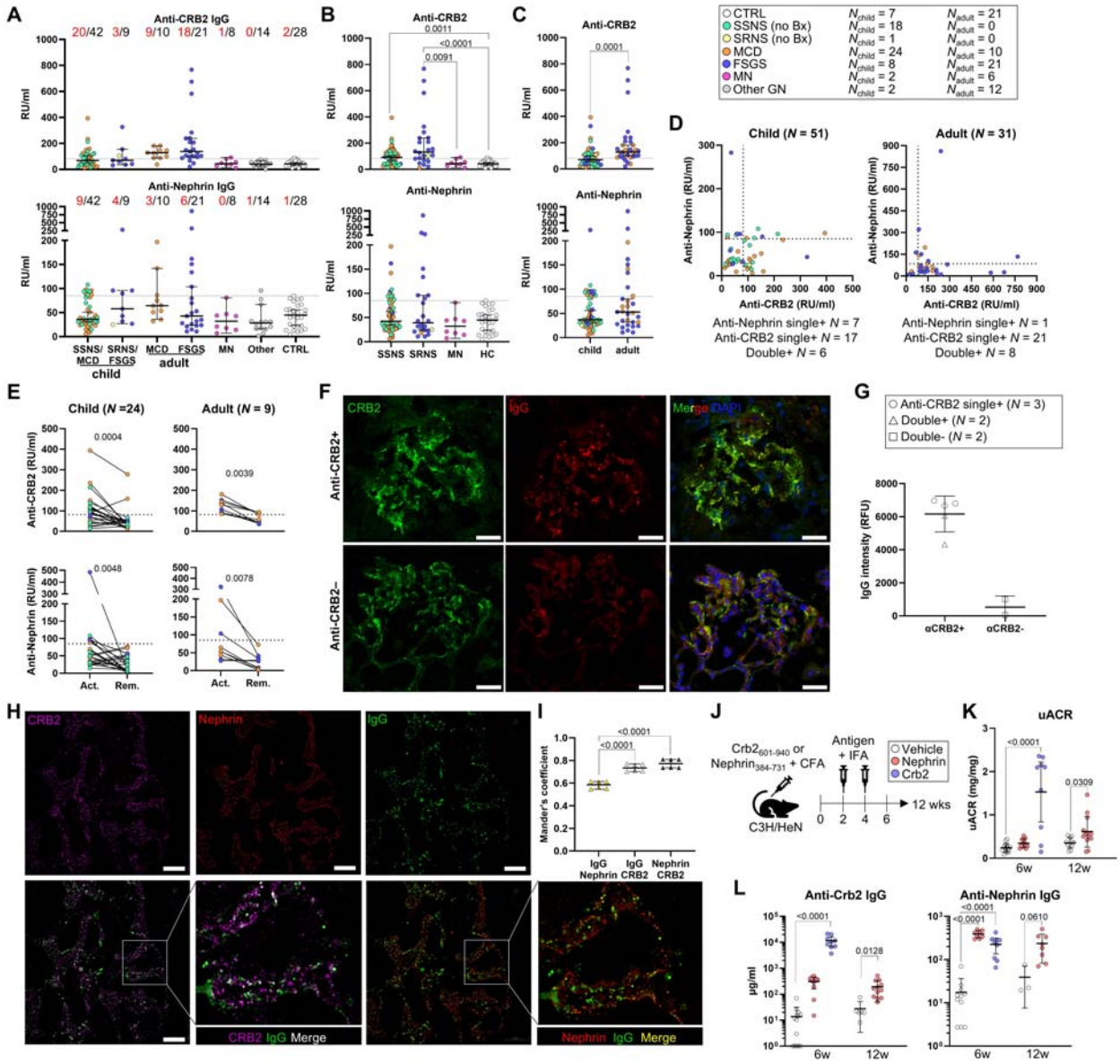

Figure 1. Anti-CRB2 autoantibodies are prevalent in idiopathic podocytopathies and can co-occur with anti-Nephrin autoantibodies. (A) Anti-CRB2 IgG and anti-Nephrin IgG titers in sera of patients with non-biopsied idiopathic nephrotic syndrome (INS, N_{child} = 21), including steroid-sensitive (SSNS, N_{child} = 20) and steroid-resistant (SRNS, N_{child} = 1), or the histological diagnoses of minimal change disease (MCD, N_{child} = 22, N_{adult} = 10), primary focal segmental

glomerulosclerosis (FSGS, N_{child} = 8, N_{adult} = 21), and membranous nephropathy (MN, N_{child} = 2, N_{adult} = 6), or other glomerular diseases (Other GN, N_{child} = 2, N_{adult} = 12) as determined by quantitative ELISA. The dotted line shows a threshold for seropositivity determined using healthy control (HC, N_{child} = 7, N_{adult} = 21) sera. The y-axis for anti-Nephrin titers is split to enhance visibility of values near the threshold. **(B)** Anti-CRB2 IgG and anti-Nephrin IgG titers for idiopathic podocytopathies divided by steroid responsiveness. **(C)** Anti-CRB2 IgG and anti-Nephrin IgG titers are compared between children and adults with idiopathic podocytopathies (SSNS, SRNS, MCD, and FSGS). **(D)** Correlations between anti-CRB2 IgG and anti-Nephrin IgG titers in children and adults with idiopathic podocytopathies. **(E)** Changes in anti-CRB2 IgG and anti-Nephrin IgG titers during active disease and remission in children (N = 24) and adults (N = 9) with idiopathic podocytopathies. **(F)** Representative glomeruli from flash frozen kidney biopsies from anti-CRB2 IgG seropositive and seronegative patients with idiopathic podocytopathies showing CRB2 (green) and IgG (red) co-localization. **(G)** Average IgG staining intensity across all glomeruli are compared between anti-CRB2 IgG seropositive (N = 5) and seronegative (N = 2) individuals. **(H)** Representative glomerulus from a single patient with both anti-CRB2 and anti-Nephrin IgG showing CRB2 (magenta) and IgG (green) or Nephrin (red) and IgG (green) co-localization visualized with high-resolution structured illumination microscopy. **(I)** Overlap between IgG and Nephrin, IgG and CRB2, and Nephrin and CRB2 calculated using the Mander's coefficient across three different areas of two glomeruli from the patient in H. **(J)** Schematic showing mouse immunization and re-challenge schedule for induction of experimental autoimmune nephrotic syndrome. **(K)** Urinary albumin-to-creatinine ratios (uACR) from immunized mice at 6-weeks and 12-weeks following immunization determined using quantitative ELISAs. **(L)** Anti-CRB2 IgG and anti-Nephrin IgG titers in

immunized mice. In all graphs, each dot represents a single patient or mouse, except in J where they represent distinct regions of a glomerulus. Summary statistics are expressed as a median with 95% confidence intervals in A-C, G, I or mean with standard deviation in K and L. *P*-values were determined using Kruskal-Wallis tests with Dunn's correction for multiple comparisons in B and I, Mann-Whitney *U*-tests in C, one-way ANOVA with Tukey's correction for multiple testing in K and L, and Wilcoxon matched-paired signed rank test in E.

Figure 2

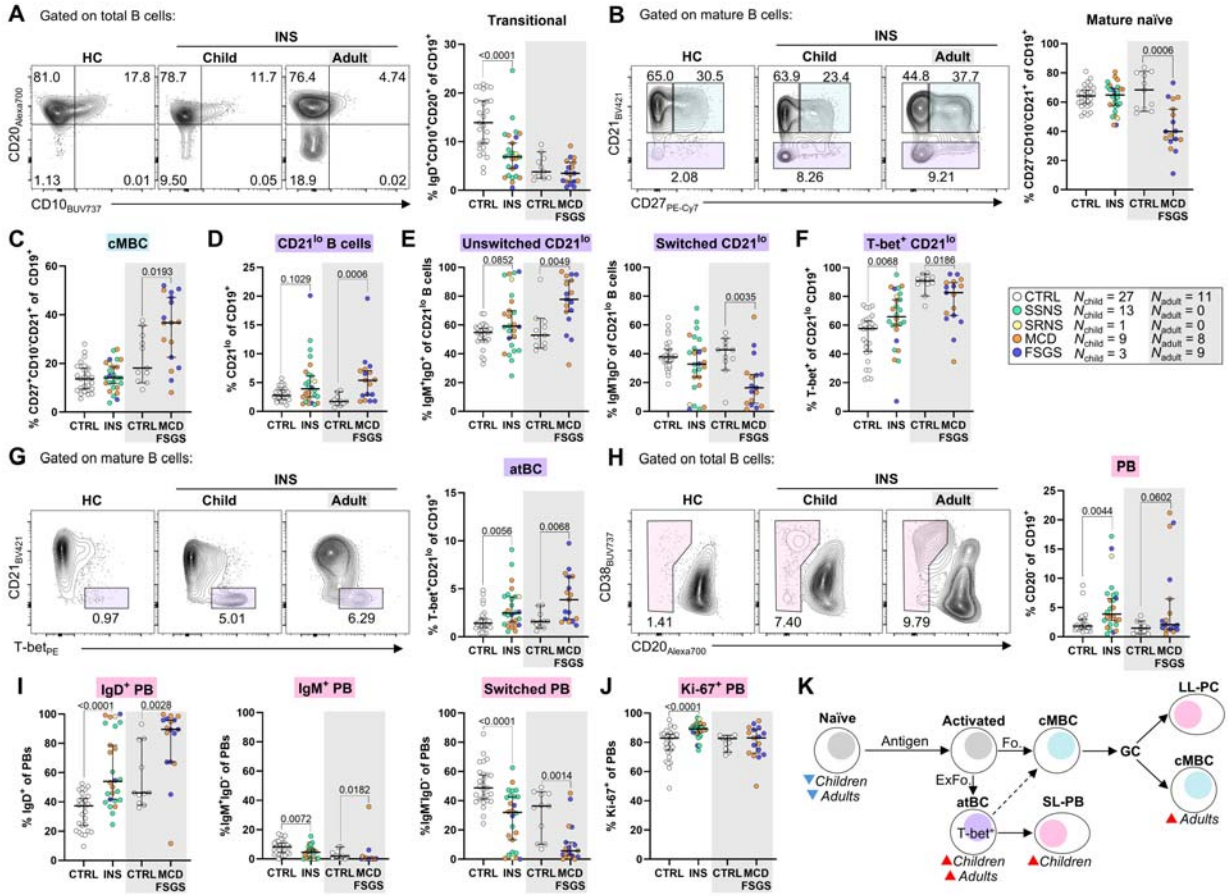

Figure 2. T-bet^{+} CD21^{low} atypical B cells and plasmablasts are expanded in children and adults with idiopathic podocytopathies. (**A**) Representative flow cytometry plots showing transitional naïve B cells (CD20^{+} CD10^{+} IgD^{+}) alongside graphs comparing their frequency within the total B cell pool in control children (N = 27), children with INS (N_{SSNS} = 15, N_{SRNS} = 1, N_{MCD} = 7, N_{FSGS} = 3), control adults (N = 11), and adults with MCD/FSGS (N_{MCD} = 8, N_{FSGS} = 9). Adult data are highlighted in gray for histograms. **(B)** Representative flow plots showing classical mature naïve B cells, classical memory B cells (cMBC, CD27^{+} CD21^{+}, in blue), and CD21^{low} B cells (CD21^{low}, in purple) alongside quantification of the frequency of mature naïve B cells amongst total B cells. **(C)** Quantification of the frequency of cMBC amongst total B cells. **(D)** Quantification of the frequency of CD21^{low} B cells amongst total B cells. **(E)** Graphs

comparing the proportions of CD21^{low} B cells that are isotype unswitched (IgM^{+} IgD^{+}) or switched (IgM^{-} IgD^{-}). **(F)** Quantification of the frequency of T-bet^{+} cells amongst CD21^{low} B cells. **(G)** Representative flow plots showing atypical B cells (atBC, T-bet^{+} CD21^{low}, in purple) alongside the quantification of their frequencies amongst total B cells. **(H)** Representative flow plots showing plasmablasts (PB, CD20^{-}, in pink) alongside quantification of their frequencies amongst total B cells. **(I)** Graphs comparing the proportions of PBs that are IgD^{+}, IgM^{+} IgD^{-}, or isotype-switched (IgM^{-} IgD^{-}). **(J)** Graph comparing the proportion of PBs that are actively cycling (Ki-67^{+}). **(K)** Diagram showing follicular (Fo.) and extrafollicular (ExFo.) B subsets and summarizing the findings of the B cell profiling. Red triangles denote increases in frequencies amongst total B cells while blue triangles denote decreases. In all graphs, points refer to a single donor and summary statistics are expressed as median with 95% confidence intervals. *P*-values were determined using Mann-Whitney *U*-tests comparing controls to patients for children and adults separately.

Figure 3

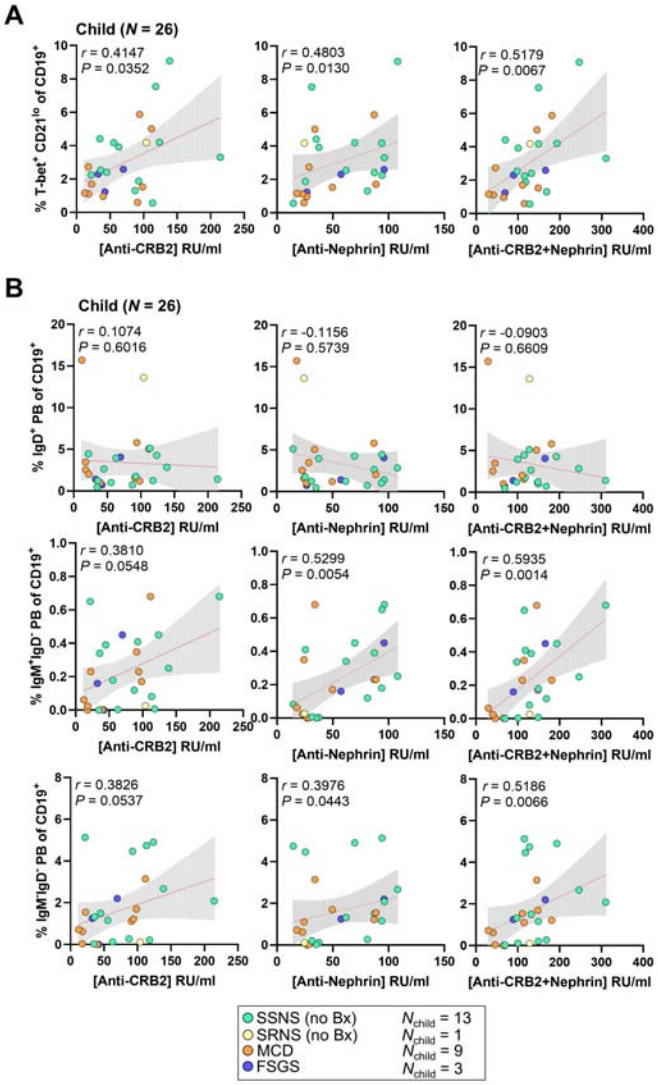

Figure 3. Atypical B cells and isotype-switched plasmablasts correlate with anti-slit diaphragm autoantibodies in children with INS. (A) Correlation between the frequency of T-bet^{+} CD21^{low} atypical B cells and serum titers of anti-CRB2 IgG, anti-Nephrin IgG, and their combined titers in children with INS (N_{SSNS} = 15, N_{SRNS} = 1, N_{MCD} = 7, N_{FSGS} = 3). **(B)** Correlation between the frequencies of IgD^{+}, IgM^{+} IgD^{-}, and IgM^{-} IgD^{-} plasmablasts (PB) and serum autoantibody titers in children with INS. In all graphs, each dot represents a single donor.

A simple linear regression line is shown alongside 95% confidence intervals for ease of visualization. Non-parametric spearman correlations were performed to obtain *r* and *P*-values.

Figure 4

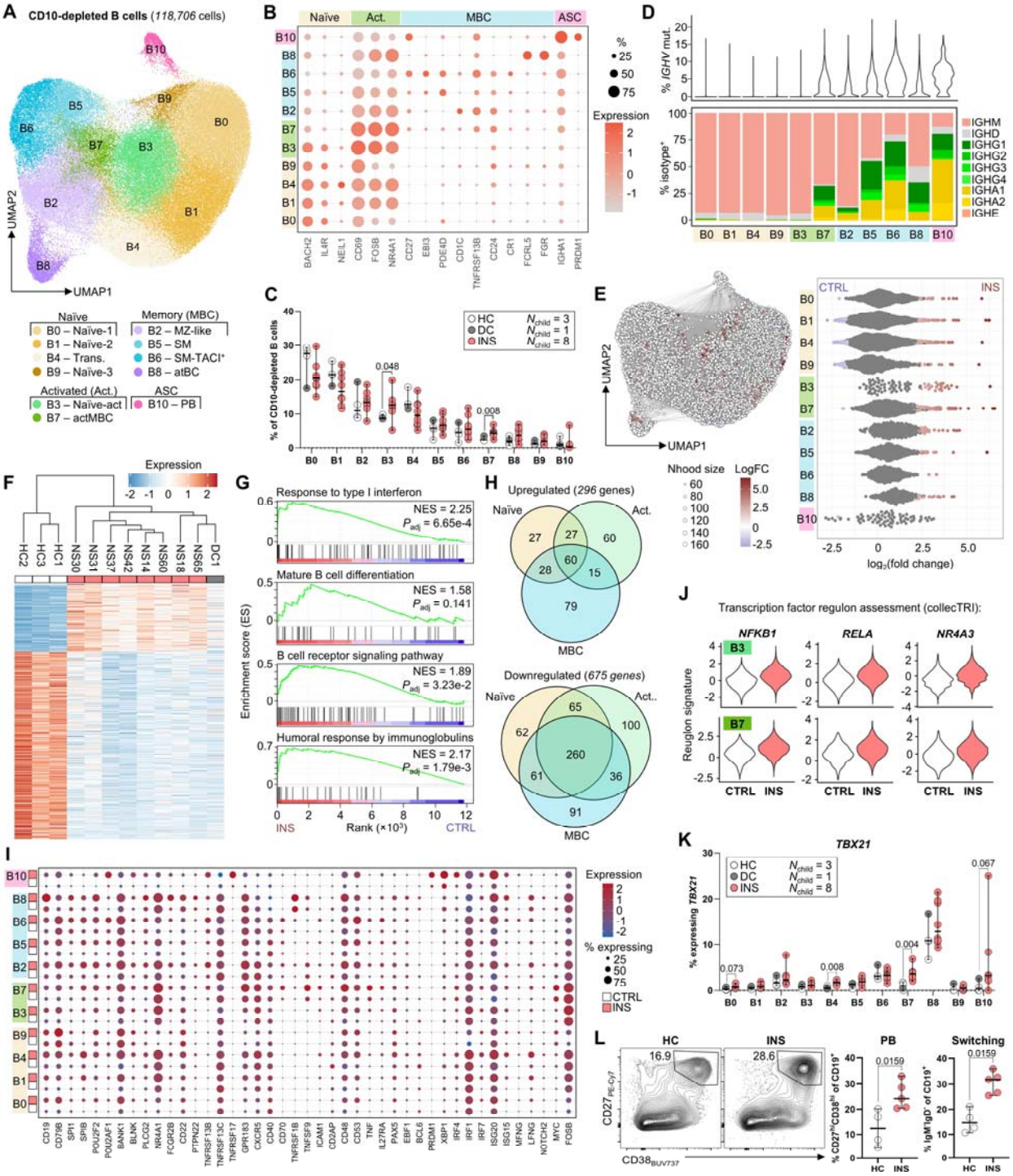

Figure 4. B cells in INS are transcriptionally poised for activation. (A) Uniform manifold approximation and projection (UMAP) plot showing naïve B cell, activated B cell (Act.),

memory B cell (MBC), and antibody-secreting cell (ASC) clusters generated from single-cell RNA-sequencing gene expression data of CD10-depleted B cells isolated from the peripheral blood of eight children with INS, three healthy controls (HC), and one atopic disease control (DC). **(B)** Bubble plot showing the expression intensity (colour-scale) and frequency (bubble size) of genes associated with naïve B cells, Act. B cells, MBCs, and ASCs across clusters. **(C)** Proportions of each B cell cluster within the dataset are shown for each donor. Each dot represents a single donor and summary statistics are represented as median with 95% confidence intervals. *P*-values were determined using independent Mann-Whitney *U*-tests between controls and INS. **(D)** A violin plot showing the distribution of somatic hypermutation, defined as the percentage of nucleotides within the *IGHV* gene that are mutated from germline, for each cluster is shown at the top. A stacked bar graph showing the prevalence of each isotype within each cluster is shown at the bottom. **(E)** Neighbourhoods determined using miloR are plotted on top of the UMAP with changes in abundance expressed as $\log_2$(fold change) alongside the quantification within each cluster. Coloured neighbourhoods are significantly (spatial $FDR < 0.1$) elevated or decreased in INS. **(F)** Heatmap showing the significantly differentially expressed genes obtained using pseudobulk differential gene expression analysis between total B cells from INS and controls. Hierarchical clustering of the donors is also shown. **(G)** Select Gene Ontology: Biological Processes terms determined to be enriched amongst INS B cells by gene-set enrichment analysis. P_{adj}-values were determined using Wilcoxon rank-sum tests with Benjamini-Hochberg corrections. **(H)** Venn diagrams showing the overlap in differentially expressed genes obtained by pseudobulk differential gene expression analysis between INS and controls for naïve B cells, Act. B cells, and MBCs. **(I)** Bubble plot comparing the expression intensity (colour-scale) and frequency (bubble size) of genes involved in B cell receptor

signaling, B cell activation, B cell differentiation, B cell homing, T/B cell crosstalk, B cell effector functions, and interferon-stimulated genes for each cluster between INS and controls. **(J)** CollecTRI regulon signatures for *NFKB1*, *RELA*, *NR4A3*, and *AP1* within the naïve-act. (B3) and actMBC (B7) clusters between control and INS. **(K)** Frequency of cells within each cluster expressing the T-bet gene *TBX21* transcripts compared between INS and controls. Each dot represents a single donor and summary statistics are represented as median with 95% confidence intervals. *P*-values were determined using independent Mann-Whitney *U*-tests between control and INS. **(L)** Total B cells isolated from peripheral blood from HC and INS children were stimulated with CD40L-Ig, anti-IgM/IgG, IL-21, and IL-4 for four days. Representative flow plots show the frequency of B cells with a plasmablast (PB, $CD38^{high}$ $CD27^{high}$) phenotype on day four alongside the quantification. Frequencies of cells that are isotype-switched are also shown. Each dot represents a single donor and summary statistics are represented as median with 95% confidence intervals. *P*-values were determined using independent Mann-Whitney *U*-tests between HC and INS.

Figure 5

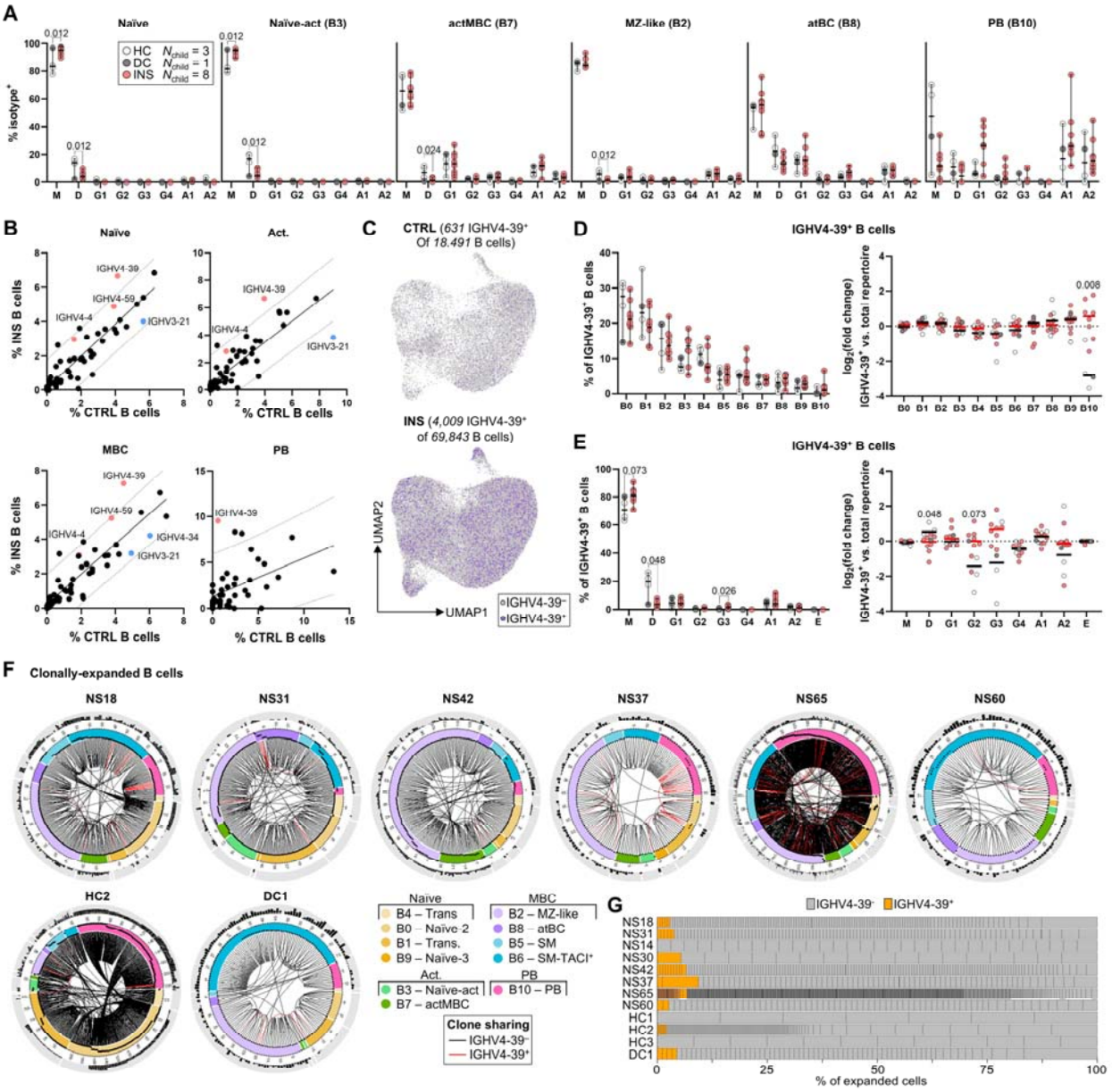

Figure 5. V_H4-39$^+$ B cell clones are abundant in INS and persist to the plasmablast pool. (A) Frequency of BCR isotype amongst all naïve B cells, activated naïve B cells (naïve-act, B3), activated memory B cells (actMBC, B7), marginal zone-like B cells (MZ-like B, B2), atypical B cells (atBC, B8), and plasmablasts (PB, B10) is compared between INS and controls (healthy

control, HC; disease control, DC). **(B)** Correlation of the usage frequency of each *IGHV* gene captured within the dataset between INS and controls for naïve B cells, activated B cells (Act.), memory B cells (MBC), and PBs. Genes highlighted in red are significantly upregulated in INS and genes highlighted in blue are significantly downregulated in INS. Each dot represents an *IGHV* gene. Simple linear regression line is provided with 95% prediction bands for visualization. **(C)** Uniform manifold approximation and projection (UMAP) showing $V_H4\text{-}39^+$ B cells in controls and INS as purple points. **(D)** Proportions of each cluster within the $V_H4\text{-}39^+$ B cell pool are shown on the left. The change in frequency of each cluster between the complete repertoire and the $V_H4\text{-}39^+$ repertoire are shown as $\log_2$(fold change) on the right. **(E)** Similarly, proportions of each isotype within the $V_H4\text{-}39^+$ B cell pool are shown on the left. The change in the frequency of each isotype between the complete repertoire and the $V_H4\text{-}39^+$ repertoire are shown as $\log_2$(fold change) on the right. **(F)** Circos plots of clonally expanded cells from the six children with INS and two control children with high levels of clonal expansion. Cells are arranged by cluster from highest to lowest degree of clonal expansion (clockwise). The outer ring shows the proportion of somatic hypermutation (ring thickness represents 20% of nucleotides mutated in the *IGHV* gene segment). Lines in the middle link cells derived from the same clone with black lines indicating IGHV4-39$^-$ clones and red lines denoting IGHV4-39$^+$ clones. **(G)** Stacked bar plots showing the proportion of clonally expanded clones. $V_H4\text{-}39^+$ clones are coloured in orange. In A, D, and E, each dot represents a single donor with summary statistics represented as median with 95% confidence intervals. *P*-values were determined using independent Mann-Whitney *U*-tests comparing INS and controls.

SUPPLEMENTAL FIGURE LEGENDS

Supplemental Figure 1

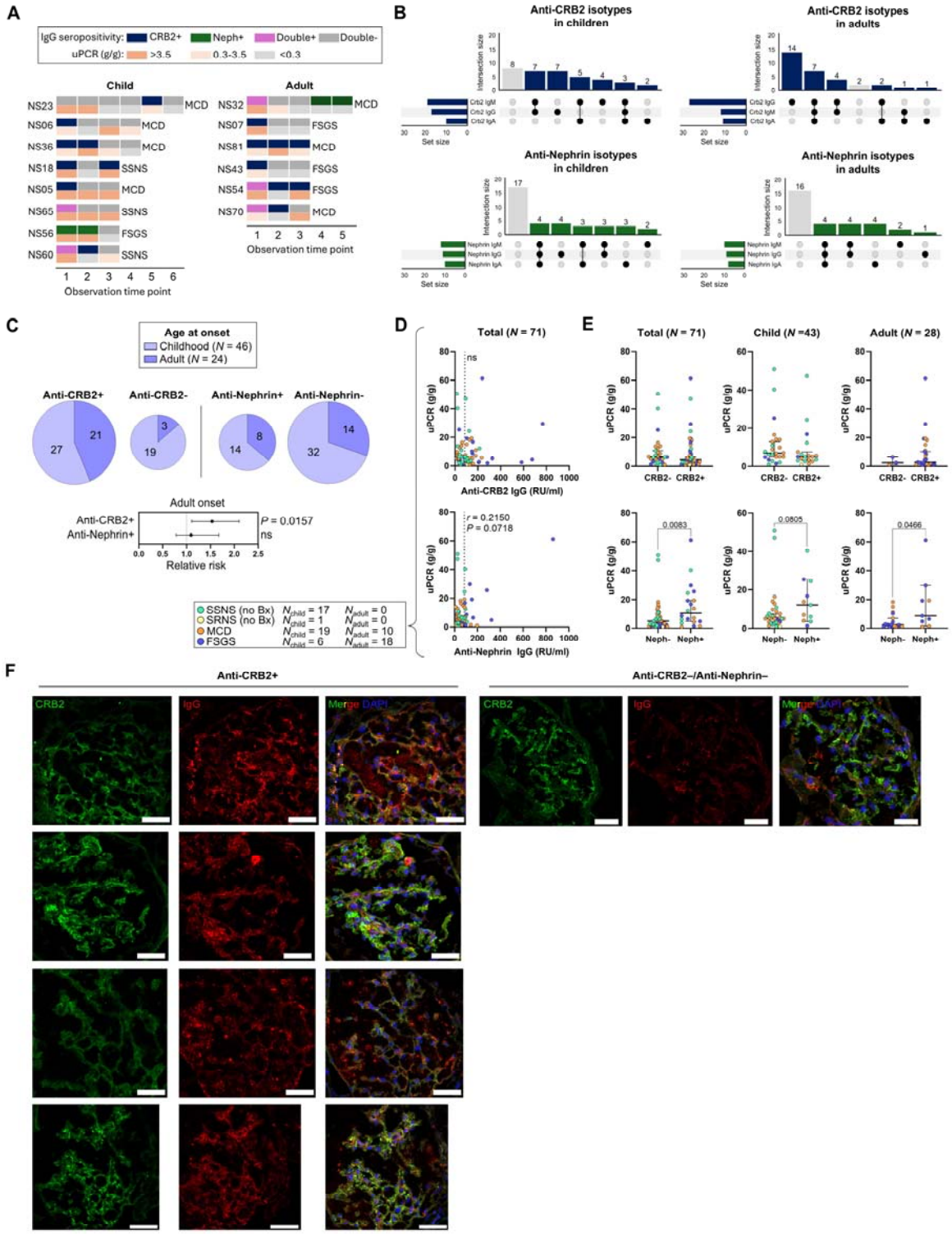

Supplemental Figure 1. Temporal evolution, isotype profile, and clinical correlates of anti-CRB2 and anti-Nephrin autoantibodies. (A) Timeline of autoantibody seropositivity status and proteinuria severity measured with the protein-to-creatinine ratio (uPCR in g/g) in patients with samples available at three or more independent clinical visits. **(B)** Upset plot showing overall seropositivity for IgG, IgM and IgA isotypes for anti-CRB2 (in blue) and anti-Nephrin (in green) autoantibodies for children (left) and adults (right). For each subgroup, vertical histograms show the number of patients seropositive for each isotype combination while horizontal histograms show the total number of patients seropositive for each isotype. **(C)** Proportion of patients with disease onset in childhood or adulthood stratified by autoantibody seropositivity. The size of each pie chart is proportional to the number of individuals captured in that group. Forest plots of the relative risk for adulthood onset given anti-CRB2 or anti-Nephrin seropositivity is plotted below the pie charts. **(D)** Correlation of uPCR and IgG autoantibody titers in patients with non-biopsied idiopathic nephrotic syndrome (INS, N_{child} = 18), including steroid-sensitive (SSNS, N_{child} = 17) and steroid-resistant (SRNS, N_{child} = 1), or the histological diagnoses of minimal change disease (MCD, N_{child} = 19, N_{adult} = 10) and primary focal segmental glomerulosclerosis (FSGS, N_{child} = 6, N_{adult} = 18). **(E)** Comparison of uPCR in autoantibody seropositive or seronegative donors shown for the total cohort or for children and adults independently. **(F)** Representative glomeruli from flash frozen kidney biopsies from the remaining four anti-CRB2 IgG seropositive patients and one seronegative patient present in the quantification in Figure 1G showing CRB2 (green) and IgG (red) co-localization. In D and E, each dot represents a single donor, and summary statistics are shown as median with 95% confidence intervals. *P*-values were determined using Fisher's exact tests in C, non-parametric Spearman correlation in D, and Mann-Whitney *U*-tests in E. This Supplemental Figure is associated with Figure 1.

Supplemental Figure 2

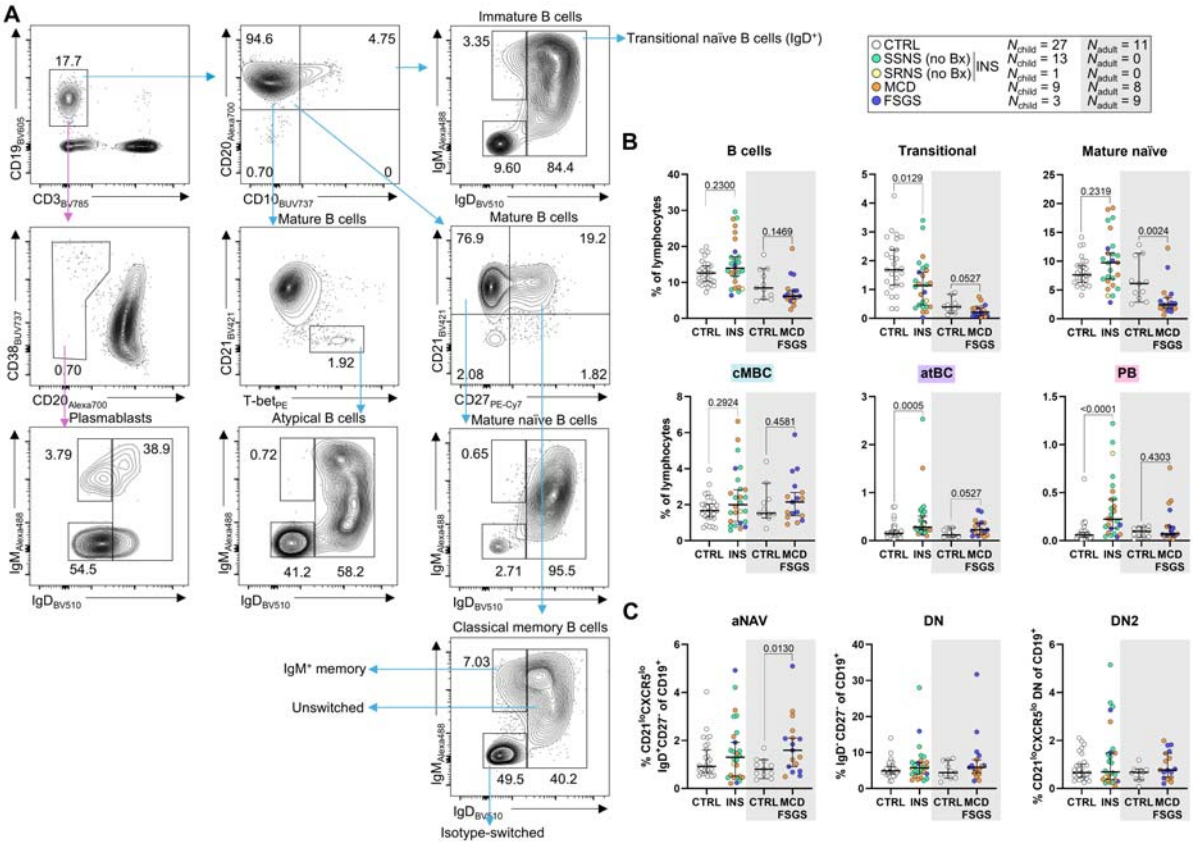

Supplemental Figure 2. Gating strategy for peripheral blood B cell populations. (A) Gating strategy for the B cell populations evaluated in this study. Total B cells ($CD19^+$) were gated from live lymphocytes and divided into mature B cells ($CD10^-$), immature B cells ($CD10^+$), and plasmablasts ($CD20^-$). Transitional naïve B cells were defined as IgD^+ immature B cells. The mature B cells were subsequently divided into mature naïve B cells ($CD27^-$ $CD21^+$), classical memory B cells (cMBC, $CD27^+$ $CD21^+$), and atypical B cells (atBC, $CD21^{low}$ T-bet$^+$). Each of population was then assessed for class-switching based on surface IgM and IgD expression. **(B)** Graphs comparing the frequencies of total B cells, transitional naïve B cells, mature B cells, cMBCs, atBCs, and plasmablasts within the total lymphocyte pool from control children (N = 27), children with INS (N_{SSNS} = 15, N_{SRNS} = 1, N_{MCD} = 7, N_{FSGS} = 3), control adults (N = 11), and

adults with MCD/FSGS (N_{MCD} = 8, N_{FSGS} = 9). Adult data are highlighted in gray for histograms. **(C)** Graphs comparing the frequencies of activated naïve B cells (aNAV, IgD^+ $CD27^-$ $CXCR5^{low}$ $CD21^{low}$), double-negative B cells (DN, IgD^- $CD27^-$) and DN2 B cells ($CXCR5^{low}$ $CD21^{low}$) within the total $CD19^+$ B cell pool. In B and C, each point refers to a single donor. Summary statistics are expressed as median with 95% confidence intervals. *P*-values were determined using Mann-Whitney *U*-tests comparing controls to patients for children and adults separately. This Supplemental Figure is associated with Figure 2.

Supplemental Figure 3

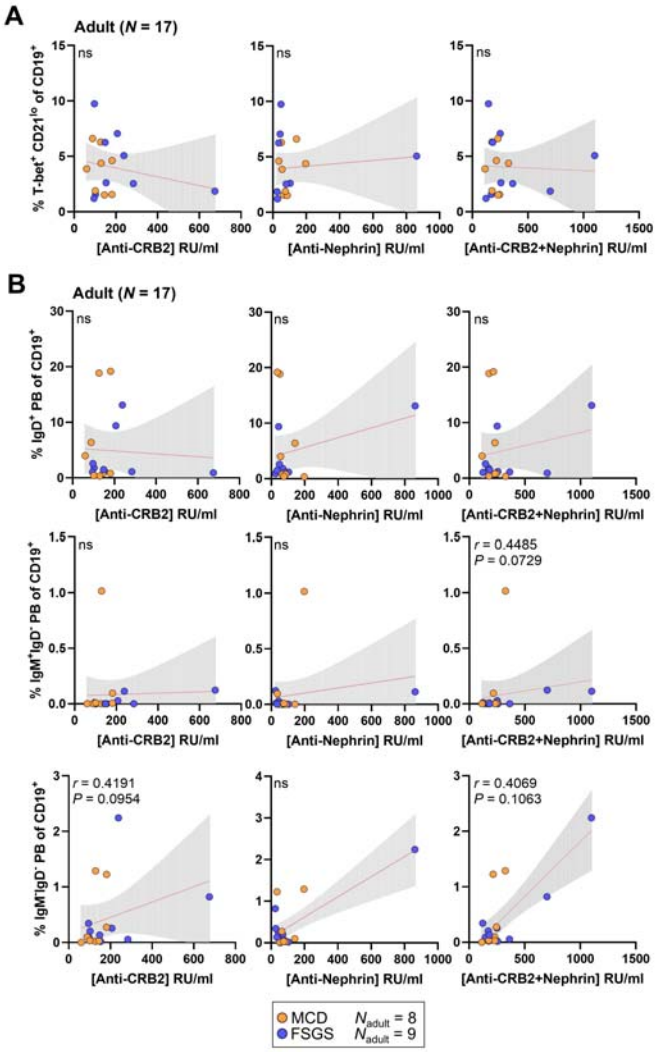

Supplemental Figure 3. Correlation between B cells and autoantibodies in adults. (A) Correlation between the frequency of T-bet^{+} CD21^{low} atypical B cells (atBC) and serum titers of anti-CRB2 IgG, anti-Nephrin IgG, and their combined titers in adults with idiopathic podocytopathies (N_{MCD} = 8, N_{FSGS} =9). **(B)** Correlation between the frequencies of IgD^{+}, IgM^{+} IgD^{-}, and IgM^{-} IgD^{-} plasmablasts (PB) and serum autoantibody titers in adults with idiopathic podocytopathies. In all graphs, each dot represents a single donor. A simple linear regression line is shown alongside 95% confidence intervals for each of visualization. Non-parametric

Spearman correlations were performed to obtain *r* and *P*-values. This Supplemental Figure is associated with Figure 3.

Supplemental Figure 4

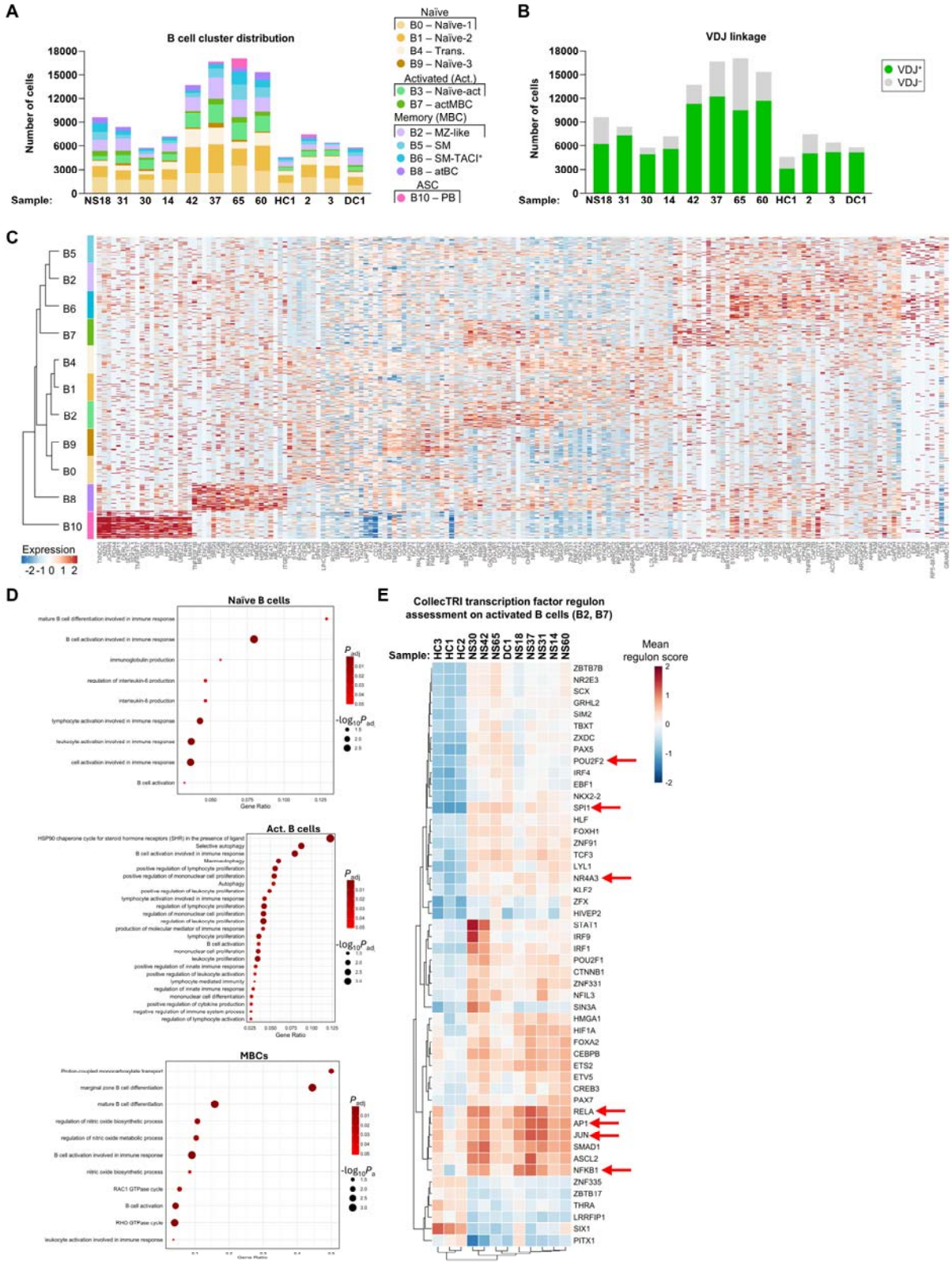

Supplemental Figure 4. Single-cell RNA-sequencing quality control, cluster markers, pathway analysis, and CollecTRI regulon scores. (A) Stacked bar graphs showing sample-level distribution of B cells from the single-cell RNA-sequencing dataset stratified by cluster. **(B)** Stacked bar graphs showing sample-level distribution of B cells from the single-cell RNA-sequencing dataset stratified by having paired VDJ sequences. **(C)** Heatmap of the top 20 expressed genes by each of the B cell clusters. **(D)** All Gene Ontology Biological Processes or REACTOME terms that are significantly over-represented in naïve B cells, activated B cells (Act.), and memory B cells (MBCs) from INS in comparison to healthy controls. Pathway analysis was conducted using g:Profiler. **(E)** Heatmap showing the mean regulon scores for CollecTRI transcription factor regulons determined using the decoupleR package from activated B cells. Shown are the top 50 regulons that are differentially present in children with idiopathic nephrotic syndrome (INS) versus controls. This Supplemental Figure is associated with Figure 4.

Supplemental Figure 5

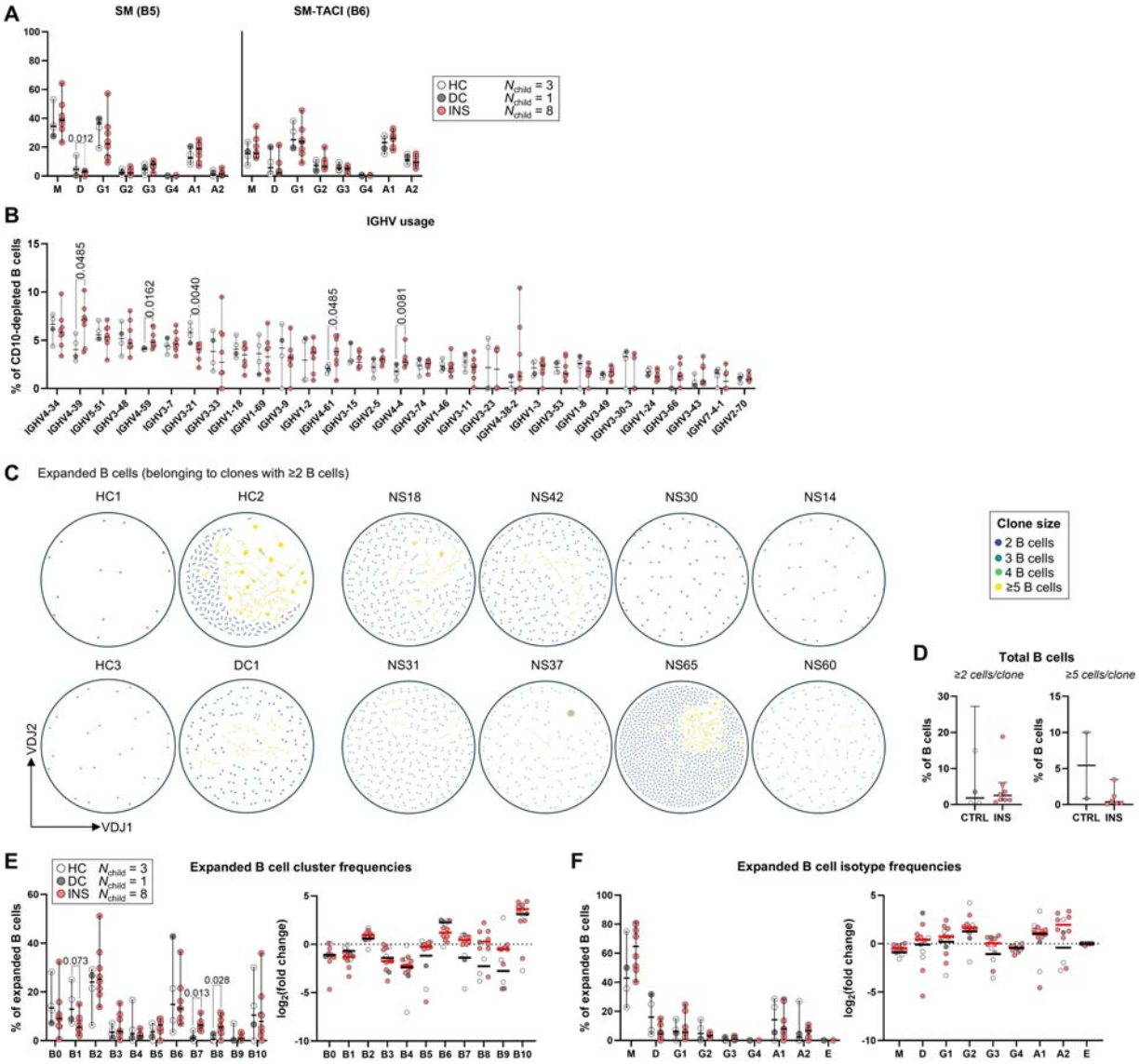

Supplemental Figure 5. Immunoglobulin gene usage and clonality in children with INS. (A) Frequency of BCR isotypes amongst switched memory (SM, cluster B5) and switched memory TACI-expressing (SM-TACI, cluster B6) B cells is compared between idiopathic nephrotic syndrome (INS) donors and controls (healthy control, HC; disease control, DC). The remaining clusters are shown in Figure 5A. **(B)** Comparison of the percentage of CD10-depleted B cells that are using each *IGHV* gene in INS and controls. Only *IGHV* genes expressed within at least

1% of total B cells are depicted. **(C)** Dandelion plots of clonally expanded B cells (i.e. clonotypes containing at least two B cells) from each control and INS donor. Each point represents a single B cell with connecting lines representing shared clonotype. **(D)** Proportion of total B cells within the single-cell RNA-sequencing dataset that are clonally expanded (at least two B cells within the clonotype) or highly expanded (at least five B cells within the clonotype) in INS donors and controls. **(E)** Comparisons of the proportions of each B cell cluster within the clonally expanded B cell pool between INS and controls are shown in the left graph. Log_2(fold change) calculated from the frequency of each B cell cluster within the clonally expanded B cell pool compared to their frequency within the entire B cell pool are shown in the right graph and compared between INS and controls. **(F)** Comparisons of the proportion of each BCR isotype within the clonally expanded B cell pool between INS and controls are shown in the left graph. Log_2(fold change) calculated from the frequency of BCR isotype within the clonally expanded B cell pool compared to their frequency within the entire B cell pool are shown in the right graph and compared between INS and controls. In A, B, D, E, and F, each dot represents a single patient with summary statistics represented as median with 95% confidence intervals. *P*-values were determined using independent Mann-Whitney *U*-tests between INS and controls. This Supplemental Figure is associated with Figure 5.

Supplemental Table 1. Patient characteristics. This table lists all the patients included in the study and their characteristics. The manuscript code is the anonymized ID of each patient included in this manuscript. The diagnosis column represents the disease with which the patient was diagnosed, where INS denotes unbiopsied idiopathic nephrotic syndrome, SSNS = steroid-sensitive INS, SRNS = steroid-resistant INS, MCD = minimal change disease, FSGS = primary

focal segmental glomerulosclerosis, MN = membranous nephropathy, IgAN = IgA nephropathy, GEN = genetic disease, C3GN = C3 glomerulonephritis, FIB = fibrillary glomerulonephritis, A-GBM = anti-glomerular basement membrane disease, AHUS = atypical hemolytic uremic syndrome, MGRS = monoclonal gammopathy of renal significance, PGNMID = proliferative glomerulonephritis with monoclonal immune deposits, and SLE = systemic lupus erythematosus. Steroid responsiveness denotes if patients were steroid-sensitive (SSNS) or resistant (SRNS). Sample date represents the date of collection of the first tested sample for each patient. The age column denotes the age of each patient at the time of sample collection. For the sex, F = female and M = male. The nest three columns describe the treatments received by each patient: if they were receiving steroids at the time of sample collection and the treatment duration, if they were receiving any other immunosuppressive agents at the time of sample collection (MMF = mycolphenolate mofetil, RTX = rituximab), and if they were previously exposed to RTX before sample collection. Disease status includes active disease, defined as proteinuria >1 g/day and/or a diagnosis of relapse by the attending nephrologist, and remission, defined as proteinuria <0.3 g/day and/or diagnosis of remission by the nephrologist (more details are provided in the Methods section). uPCR denotes urinary protein-to-creatinine ratio, measured here in g/g. The next four columns state the anti-CRB2 and the anti-Nephrin autoantibody titer in µg/mL and the associated interpretation (seropositivity or seronegativity). The final columns titled IgM/IgA isotyping, Confocal, Super resolution, Flow cytometry, scRNAseq (single-cell RNA-sequencing), and *in vitro* plasmablast differentiation indicates the patients that were included in each of these analyses.

REFERENCES

Al-Aubodah, T.-A., L. Aoudjit, G. Pascale, M.A. Perinpanayagam, D. Langlais, M. Bitzan, S.M. Samuel, C.A. Piccirillo, and T. Takano. 2023. The extrafollicular B cell response is a hallmark of childhood idiopathic nephrotic syndrome. *Nature Communications* 14:7682.

Al-Aubodah, T.-A., C.A. Piccirillo, H. Trachtman, and T. Takano. 2025. The autoimmune architecture of childhood idiopathic nephrotic syndrome. *Kidney International* 107:271-279.

Ambegaonkar, A.A., P. Holla, B.L.P. Dizon, H. Sohn, and S.K. Pierce. 2022. Atypical B cells in chronic infectious diseases and systemic autoimmunity: puzzles with many missing pieces. *Current Opinion in Immunology* 77:102227.

Anders, H.-J., A.R. Kitching, N. Leung, and P. Romagnani. 2023. Glomerulonephritis: immunopathogenesis and immunotherapy. *Nature Reviews Immunology* 23:453-471.

Barry, A., M.T. McNulty, X. Jia, Y. Gupta, H. Debiec, Y. Luo, C. Nagano, T. Horinouchi, S. Jung, M. Colucci, D.F. Ahram, A. Mitrotti, A. Sinha, N. Teeninga, G. Jin, S. Shril, G. Caridi, M. Bodria, T.Y. Lim, R. Westland, F. Zanoni, M. Marasa, D. Turudic, M. Giordano, L. Gesualdo, R. Magistroni, I. Pisani, E. Fiaccadori, J. Reiterova, S. Maringhini, W. Morello, G. Montini, P.L. Weng, F. Scolari, M. Saraga, V. Tasic, D. Santoro, J.A.E. van Wijk, D. Milošević, Y. Kawai, K. Kiryluk, M.R. Pollak, A. Gharavi, F. Lin, A.C. Simœs e Silva, R.J.F. Loos, E.E. Kenny, M.F. Schreuder, A. Zurowska, C. Dossier, G. Ariceta, M. Drozynska-Duklas, J. Hogan, A. Jankauskiene, F. Hildebrandt, L. Prikhodina, K. Song, A. Bagga, H. Cheong, G.M. Ghiggeri, P. Vachvanichsanong, K. Nozu, D. Lee, M. Vivarelli, S. Raychaudhuri, K. Tokunaga, S. Sanna-Cherchi, P. Ronco, K. Iijima, and M.G. Sampson. 2023. Multi-population genome-wide association study implicates immune and non-immune factors in pediatric steroid-sensitive nephrotic syndrome. *Nature Communications* 14:2481.

Bashford-Rogers, R.J.M., L. Bergamaschi, E.F. McKinney, D.C. Pombal, F. Mescia, J.C. Lee, D.C. Thomas, S.M. Flint, P. Kellam, D.R.W. Jayne, P.A. Lyons, and K.G.C. Smith. 2019. Analysis of the B cell receptor repertoire in six immune-mediated diseases. *Nature* 574:122-126.

Bashford-Rogers, R.J.M., A.L. Palser, B.J. Huntly, R. Rance, G.S. Vassiliou, G.A. Follows, and P. Kellam. 2013. Network properties derived from deep sequencing of human B-cell receptor repertoires delineate B-cell populations. *Genome Research* 23:1874-1884.

Batal, I., A.J.B. Watts, J.B. Gibier, A. Hamroun, I. Top, F. Provot, K. Keller, X. Ye, H.E. Fernandez, R. Leal, N.K. Andeen, R.J. Crew, G.K. Dube, E.R. Vasilescu, L.E. Ratner, N. Bowman, A.S. Bomback, S. Sanna-Cherchi, K. Kiryluk, and A. Weins. 2024. Pre-transplant anti-nephrin antibodies are specific predictors of recurrent diffuse podocytopathy in the kidney allograft. *Kidney Int* 106:749-752.

Beck, L.H., R.G.B. Bonegio, G. Lambeau, D.M. Beck, D.W. Powell, T.D. Cummins, J.B. Klein, and D.J. Salant. 2009. M-Type Phospholipase A_2 Receptor as Target Antigen in Idiopathic Membranous Nephropathy. *New England Journal of Medicine* 361:11-21.

Claes, N., J. Fraussen, M. Vanheusden, N. Hellings, P. Stinissen, B. Van Wijmeersch, R. Hupperts, and V. Somers. 2016. Age-Associated B Cells with Proinflammatory Characteristics Are Expanded in a Proportion of Multiple Sclerosis Patients. *J Immunol* 197:4576-4583.

Crowell, H.L., C. Soneson, P.-L. Germain, D. Calini, L. Collin, C. Raposo, D. Malhotra, and M.D. Robinson. 2020. muscat detects subpopulation-specific state transitions from multi-sample multi-condition single-cell transcriptomics data. *Nature Communications* 11:6077.

D'Agati, V.D., F.J. Kaskel, and R.J. Falk. 2011. Focal Segmental Glomerulosclerosis. *New England Journal of Medicine* 365:2398-2411.

Dann, E., N.C. Henderson, S.A. Teichmann, M.D. Morgan, and J.C. Marioni. 2022. Differential abundance testing on single-cell data using k-nearest neighbor graphs. *Nature Biotechnology* 40:245-253.

Debiec, H., C. Dossier, E. Letouzé, C.E. Gillies, M. Vivarelli, R.K. Putler, E. Ars, E. Jacqz-Aigrain, V. Elie, M. Colucci, S. Debette, P. Amouyel, S.C. Elalaoui, A. Sefiani, V. Dubois, T. Simon, M. Kretzler, J. Ballarin, F. Emma, M.G. Sampson, G. Deschênes, and P. Ronco. 2018. Transethnic, Genome-Wide Analysis Reveals Immune-Related Risk Alleles and Phenotypic Correlates in Pediatric Steroid-Sensitive Nephrotic Syndrome. *Journal of the American Society of Nephrology* 29:

Deguine, J., and R.J. Xavier. 2024. B cell tolerance and autoimmunity: Lessons from repertoires. *Journal of Experimental Medicine* 221:

Dieudonné, Y., R. Lorenzetti, J. Rottura, I. Janowska, Q. Frenger, L. Jacquel, O. Vollmer, F. Carbone, Z. Chengsong, M. Luka, S. Depauw, N. Wadier, S. Giorgiutti, B. Nespola, A. Herb, R.E. Voll, A. Guffroy, V. Poindron, M. Ménager, T. Martin, P. Soulas-Sprauel, M. Rizzi, A.-S. Korganow, and V. Gies. 2024. Defective germinal center selection results in persistence of self-reactive B cells from the primary to the secondary repertoire in Primary Antiphospholipid Syndrome. *Nature Communications* 15:9921.

Downie, M.L., S. Gupta, C. Voinescu, A.P. Levine, O. Sadeghi-Alavijeh, S. Dufek-Kamperis, J. Cao, M. Christian, J.A. Kari, S. Thalgahagoda, R. Ranawaka, A. Abeyagunawardena, R. Gbadegesin, R. Parekh, R. Kleta, D. Bockenhauer, H.C. Stanescu, and D.P. Gale. 2023. Common Risk Variants in AHI1 Are Associated With Childhood Steroid Sensitive Nephrotic Syndrome. *Kidney Int Rep* 8:1562-1574.

Dufek, S., C. Cheshire, A.P. Levine, R.S. Trompeter, N. Issler, M. Stubbs, M. Mozere, S. Gupta, E. Klootwijk, V. Patel, D. Hothi, A. Waters, H. Webb, K. Tullus, L. Jenkins, L. Godinho, E. Levtchenko, J. Wetzels, N. Knoers, N. Teeninga, J. Nauta, M. Shalaby, S. Eldesoky, J.A. Kari, S. Thalgahagoda, R. Ranawaka, A. Abeyagunawardena, A. Adeyemo, M. Kristiansen, R. Gbadegesin, N.J. Webb, D.P. Gale, H.C. Stanescu, R. Kleta, and D. Bockenhauer. 2019. Genetic Identification of Two Novel Loci Associated with Steroid-Sensitive Nephrotic Syndrome. *Journal of the American Society of Nephrology* 30:

Duty, J.A., P. Szodoray, N.-Y. Zheng, K.A. Koelsch, Q. Zhang, M. Swiatkowski, M. Mathias, L. Garman, C. Helms, B. Nakken, K. Smith, A.D. Farris, and P.C. Wilson. 2008. Functional anergy in a subpopulation of naive B cells from healthy

humans that express autoreactive immunoglobulin receptors. *Journal of Experimental Medicine* 206:139-151.

Elsner, R.A., and M.J. Shlomchik. 2020. Germinal Center and Extrafollicular B Cell Responses in Vaccination, Immunity, and Autoimmunity. *Immunity* 53:1136-1150.

Fahlquist-Hagert, C., T.R. Wittenborn, E. Terczyńska-Dyla, K.S. Kastberg, E. Yang, A.N. Rallistan, Q.R. Markett, G. Winther, S. Fonager, L.F. Voss, M.K. Pedersen, N. van Campen, A. Ferapontov, L. Jensen, J. Huang, J.D. Nieland, C.E. van der Poel, J. Palmfeldt, M.C. Carroll, P.J. Utz, Y. Luo, L. Lin, and S.E. Degn. 2023. Antigen presentation by B cells enables epitope spreading across an MHC barrier. *Nature Communications* 14:6941.

Gao, X., Q. Shen, J.A. Roco, B. Dalton, K. Frith, C.M.L. Munier, F.D. Ballard, K. Wang, H.G. Kelly, M. Nekrasov, J.-S. He, R. Jaeger, P. Carreira, J.I. Ellyard, L. Beattie, A. Enders, M.C. Cook, J.J. Zaunders, and I.A. Cockburn. 2024. Zeb2 drives the formation of $CD11c^+$ atypical B cells to sustain germinal centers that control persistent infection. *Science Immunology* 9:eadj4748.

Gatto, D., and R. Brink. 2013. B cell localization: regulation by EBI2 and its oxysterol ligand. *Trends in Immunology* 34:336-341.

Gbadegesin, R.A., A. Adeyemo, N.J.A. Webb, L.A. Greenbaum, A. Abeyagunawardena, S. Thalgahagoda, A. Kale, D. Gipson, T. Srivastava, J.-J. Lin, D. Chand, T.E. Hunley, P.D. Brophy, A. Bagga, A. Sinha, M.N. Rheault, J. Ghali, K. Nicholls, E. Abraham, H.S. Janjua, A. Omoloja, G.-M. Barletta, Y. Cai, D.D. Milford, C. O'Brien, A. Awan, V. Belostotsky, W.E. Smoyer, A. Homstad, G. Hall, G. Wu, S. Nagaraj, D. Wigfall, J. Foreman, M.P. Winn, and C. Mid-West Pediatric Nephrology. 2015. HLA-DQA1 and PLCG2 Are Candidate Risk Loci for Childhood-Onset Steroid-Sensitive Nephrotic Syndrome. *Journal of the American Society of Nephrology : JASN* 26:1701-1710.

Giudicelli, V., D. Chaume, and M.-P. Lefranc. 2005. IMGT/GENE-DB: a comprehensive database for human and mouse immunoglobulin and T cell receptor genes. *Nucleic Acids Research* 33:D256-D261.

Gounari, M., S. Ntoufa, C.C. Chu, A. Tsaftaris, N. Chiorazzi, K. Stamatopoulos, and P. Ghia. 2012. Promiscuous Antigen Reactivity May Underlie Clinical Aggressiveness and Increased Risk for Richter's Syndrome in Chronic Lymphocytic Leukemia with Stereotyped IGHV4-39/IGKV1(D)-39 B Cell Receptors. *Blood* 120:561.

Gupta, N.T., K.D. Adams, A.W. Briggs, S.C. Timberlake, F. Vigneault, and S.H. Kleinstein. 2017. Hierarchical Clustering Can Identify B Cell Clones with High Confidence in Ig Repertoire Sequencing Data. *The Journal of Immunology* 198:2489-2499.

Gupta, N.T., J.A. Vander Heiden, M. Uduman, D. Gadala-Maria, G. Yaari, and S.H. Kleinstein. 2015. Change-O: a toolkit for analyzing large-scale B cell immunoglobulin repertoire sequencing data. *Bioinformatics* 31:3356-3358.

Hada, I., A. Shimizu, H. Takematsu, Y. Nishibori, T. Kimura, T. Fukutomi, A. Kudo, N. Ito-Nitta, Z. Kiuchi, J. Patrakka, N. Mikami, S. Leclerc, Y. Akimoto, Y. Hirayama, S. Mori, T. Takano, and K. Yan. 2022. A Novel Mouse Model of Idiopathic Nephrotic Syndrome Induced by Immunization with the Podocyte Protein Crb2. *Journal of the American Society of Nephrology* 33:

Hamano, S., Y. Nishibori, I. Hada, N. Mikami, N. Ito-Nitta, D. Fukuhara, A. Kudo, Z. Xiao, M. Nukui, J. Patrakka, K. Tryggvason, and K. Yan. 2018. Association of crumbs homolog-2 with mTORC1 in developing podocyte. *PLoS One* 13:e0202400.

Hao, Y., S. Hao, E. Andersen-Nissen, W.M. Mauck, III, S. Zheng, A. Butler, M.J. Lee, A.J. Wilk, C. Darby, M. Zager, P. Hoffman, M. Stoeckius, E. Papalexi, E.P. Mimitou, J. Jain, A. Srivastava, T. Stuart, L.M. Fleming, B. Yeung, A.J. Rogers, J.M. McElrath, C.A. Blish, R. Gottardo, P. Smibert, and R. Satija. 2021. Integrated analysis of multimodal single-cell data. *Cell* 184:3573-3587.e3529.

He, Y., and C.G. Vinuesa. 2024. Chapter Four - Germinal center versus extrafollicular responses in systemic autoimmunity: Who turns the blade on self? In Advances in Immunology. F.W. Alt, and K.M. Murphy, editors. Academic Press, 109-133.

Hengel, F.E., S. Dehde, M. Lassé, G. Zahner, L. Seifert, A. Schnarre, O. Kretz, F. Demir, H.O. Pinnschmidt, F. Grahammer, R. Lucas, L.M. Mehner, T. Zimmermann, A.M. Billing, J. Oh, A. Mitrotti, P. Pontrelli, H. Debiec, C. Dossier, M. Colucci, F. Emma, W.E. Smoyer, A. Weins, F. Schaefer, N. Alachkar, A. Diemert, J. Hogan, E. Hoxha, T. Wiech, M.M. Rinschen, P. Ronco, M. Vivarelli, L. Gesualdo, N.M. Tomas, and T.B. Huber. 2024. Autoantibodies Targeting Nephrin in Podocytopathies. *New England Journal of Medicine* 0:

Hertig, A., D. Droz, P. Lesavre, J.-P. Grünfeld, and P. Rieu. 2002. SLE and idiopathic nephrotic syndrome: Coincidence or not? *American Journal of Kidney Diseases* 40:1179-1184.

Hoehn, K.B., O.G. Pybus, and S.H. Kleinstein. 2022. Phylogenetic analysis of migration, differentiation, and class switching in B cells. *PLOS Computational Biology* 18:e1009885.

Holla, P., B. Dizon, A.A. Ambegaonkar, N. Rogel, E. Goldschmidt, A.K. Boddapati, H. Sohn, D. Sturdevant, J.W. Austin, L. Kardava, L. Yuesheng, P. Liu, S. Moir, S.K. Pierce, and A. Madi. 2021. Shared transcriptional profiles of atypical B cells suggest common drivers of expansion and function in malaria, HIV, and autoimmunity. *Sci Adv* 7:

Hu, W., Y. Chen, S. Wang, H. Chen, Z. Liu, C. Zeng, H. Zhang, and Z. Liu. 2016. Clinical-Morphological Features and Outcomes of Lupus Podocytopathy. *Clin J Am Soc Nephrol* 11:585-592.

Jenks, S.A., K.S. Cashman, M.C. Woodruff, F.E. Lee, and I. Sanz. 2019. Extrafollicular responses in humans and SLE. *Immunol Rev* 288:136-148.

Jenks, S.A., K.S. Cashman, E. Zumaquero, U.M. Marigorta, A.V. Patel, X. Wang, D. Tomar, M.C. Woodruff, Z. Simon, R. Bugrovsky, E.L. Blalock, C.D. Scharer, C.M. Tipton, C. Wei, S.S. Lim, M. Petri, T.B. Niewold, J.H. Anolik, G. Gibson, F.E. Lee, J.M. Boss, F.E. Lund, and I. Sanz. 2018. Distinct Effector B Cells Induced by Unregulated Toll-like Receptor 7 Contribute to Pathogenic Responses in Systemic Lupus Erythematosus. *Immunity* 49:725-739.e726.

KDIGO. 2021. KDIGO 2021 Clinical Practice Guideline for the Management of Glomerular Diseases. *Kidney Int* 100:S1-s276.

Kopp, J.B., H.-J. Anders, K. Susztak, M.A. Podestà, G. Remuzzi, F. Hildebrandt, and P. Romagnani. 2020. Podocytopathies. *Nature Reviews Disease Primers* 6:68.

Laidlaw, B.J., and J.G. Cyster. 2021. Transcriptional regulation of memory B cell differentiation. *Nature Reviews Immunology* 21:209-220.

Maas, R.J., J.K. Deegens, B. Smeets, M.J. Moeller, and J.F. Wetzels. 2016. Minimal change disease and idiopathic FSGS: manifestations of the same disease. *Nature Reviews Nephrology* 12:768-776.

Möller-Kerutt, A., J.E. Rodriguez-Gatica, K. Wacker, R. Bhatia, J.-P. Siebrasse, N. Boon, V. Van Marck, P. Boor, U. Kubitscheck, J. Wijnholds, H. Pavenstädt, and T. Weide. 2021. Crumbs2 Is an Essential Slit Diaphragm Protein of the Renal Filtration Barrier. *Journal of the American Society of Nephrology* 32:

Mueller, J., M. Matloubian, and J. Zikherman. 2015. Cutting Edge: An In Vivo Reporter Reveals Active B Cell Receptor Signaling in the Germinal Center. *The Journal of Immunology* 194:2993-2997.

Müller-Dott, S., E. Tsirvouli, M. Vazquez, Ricardo O. Ramirez Flores, P. Badia-i-Mompel, R. Fallegger, D. Türei, A. Lægreid, and J. Saez-Rodriguez. 2023. Expanding the coverage of regulons from high-confidence prior knowledge for accurate estimation of transcription factor activities. *Nucleic Acids Research* 51:10934-10949.

Mumtaz, I.M., B.F. Hoyer, D. Panne, K. Moser, O. Winter, Q.Y. Cheng, T. Yoshida, G.-R. Burmester, A. Radbruch, R.A. Manz, and F. Hiepe. 2012. Bone marrow of NZB/W mice is the major site for plasma cells resistant to dexamethasone and cyclophosphamide: Implications for the treatment of autoimmunity. *Journal of Autoimmunity* 39:180-188.

Nouri, N., and S.H. Kleinstein. 2018. A spectral clustering-based method for identifying clones from high-throughput B cell repertoire sequencing data. *Bioinformatics* 34:i341-i349.

Pugh-Bernard, A.E., G.J. Silverman, A.J. Cappione, M.E. Villano, D.H. Ryan, R.A. Insel, and I. Sanz. 2001. Regulation of inherently autoreactive VH4-34 B cells in the maintenance of human B cell tolerance. *J Clin Invest* 108:1061-1070.

Raglianti, V., M.L. Angelotti, L. Cirillo, F. Ravaglia, S. Landini, V. Palazzo, M.E. Melica, G. Antonelli, C. Conte, E. Buti, C. Errichiello, L. De Chiara, A.J. Peired, L. Lasagni, A.M. Buccoliero, M. Allinovi, A.M. Montero, J.M. Cruzado, M. Bruschi, G.M. Ghiggeri, A. Angeletti, H.J. Anders, E. Lazzeri, B. Mazzinghi, F. Becherucci, and P. Romagnani. 2024. Anti-slit diaphragm antibodies on kidney biopsy identify pediatric patients with steroid-resistant nephrotic syndrome responsive to second-line immunosuppressants. *Kidney Int* 106:1124-1134.

Raglianti, V., M.L. Angelotti, L. De Chiara, M. Allinovi, L. Cirillo, A. Manonelles, J.M. Cruzado, M.E. Melica, G. Antonelli, C. Conte, A.J. Peired, L. Lasagni, B. Lange-Sperandio, H.-J. Anders, F. Becherucci, E. Lazzeri, B. Mazzinghi, and P. Romagnani. 2025. Anti-slit Antibodies against Podocin and Kirrel1 in Pediatric and Adult Podocytopathies. *Journal of the American Society of Nephrology* 36:702-705.

Ravani, P., A. Bonanni, R. Rossi, G. Caridi, and G.M. Ghiggeri. 2016. Anti-CD20 Antibodies for Idiopathic Nephrotic Syndrome in Children. *Clin J Am Soc Nephrol* 11:710-720.

Richardson, C., A.S. Chida, D. Adlowitz, L. Silver, E. Fox, S.A. Jenks, E. Palmer, Y. Wang, J. Heimburg-Molinaro, Q.Z. Li, C. Mohan, R. Cummings, C. Tipton, and I.

Sanz. 2013. Molecular basis of 9G4 B cell autoreactivity in human systemic lupus erythematosus. *J Immunol* 191:4926-4939.

Sabouri, Z., S. Perotti, E. Spierings, P. Humburg, M. Yabas, H. Bergmann, K. Horikawa, C. Roots, S. Lambe, C. Young, T.D. Andrews, M. Field, A. Enders, J.H. Reed, and C.C. Goodnow. 2016. IgD attenuates the IgM-induced anergy response in transitional and mature B cells. *Nat Commun* 7:13381.

Samuel, S., S. Scott, C. Morgan, A. Dart, C. Mammen, R. Parekh, A. Nettel-Aguirre, A. Eddy, R. Flynn, M. Pinsk, A. Wade, S. Arora, G. Benoit, M. Bitzan, R. Erickson, J. Feber, G. Filler, P. Geier, C. Girardin, S. Grisaru, J. Tee, K. Kemp, and M. Zappitelli. 2014. The Canadian Childhood Nephrotic Syndrome (CHILDNEPH) Project: overview of design and methods. *Canadian Journal of Kidney Health and Disease* 1:17.

Shirai, Y., K. Miura, K. Ishizuka, T. Ando, S. Kanda, J. Hashimoto, Y. Hamasaki, K. Hotta, N. Ito, K. Honda, K. Tanabe, T. Takano, and M. Hattori. 2024. A multi-institutional study found a possible role of anti-nephrin antibodies in post-transplant focal segmental glomerulosclerosis recurrence. *Kidney International* 105:608-617.

Sinha, A., and A. Bagga. 2013. Rituximab therapy in nephrotic syndrome: implications for patients' management. *Nature Reviews Nephrology* 9:154-169.

Siu, J.H.Y., M.J. Pitcher, T.J. Tull, R.L. Velounias, W. Guesdon, L. Montorsi, K.T. Mahbubani, R. Ellis, P. Dhami, K. Todd, U.D. Kadolsky, M. Kleeman, D.P. D'Cruz, K. Saeb-Parsy, M. Bemark, G.J. Pettigrew, and J. Spencer. 2022. Two subsets of human marginal zone B cells resolved by global analysis of lymphoid tissues and blood. *Science Immunology* 7:eabm9060.

Slavotinek, A., J. Kaylor, H. Pierce, M. Cahr, Stephanie J. DeWard, D. Schneidman-Duhovny, A. Alsadah, F. Salem, G. Schmajuk, and L. Mehta. 2015. CRB2 Mutations Produce a Phenotype Resembling Congenital Nephrosis, Finnish Type, with Cerebral Ventriculomegaly and Raised Alpha-Fetoprotein. *The American Journal of Human Genetics* 96:162-169.

Su, Z., Y. Jin, Y. Zhang, Z. Guan, H. Li, X. Chen, C. Xie, C. Zhang, X. Liu, P. Li, P. Ye, L. Zhang, Y. Kong, and W. Luo. 2021. The Diagnostic and Prognostic Potential of the B-Cell Repertoire in Membranous Nephropathy. *Front Immunol* 12:635326.

Suo, C., K. Polanski, E. Dann, R.G.H. Lindeboom, R. Vilarrasa-Blasi, R. Vento-Tormo, M. Haniffa, K.B. Meyer, L.M. Dratva, Z.K. Tuong, M.R. Clatworthy, and S.A. Teichmann. 2024. Dandelion uses the single-cell adaptive immune receptor repertoire to explore lymphocyte developmental origins. *Nature Biotechnology* 42:40-51.

Sutton, H.J., R. Aye, A.H. Idris, R. Vistein, E. Nduati, O. Kai, J. Mwacharo, X. Li, X. Gao, T.D. Andrews, M. Koutsakos, T.H.O. Nguyen, M. Nekrasov, P. Milburn, A. Eltahla, A.A. Berry, N. Kc, S. Chakravarty, B.K.L. Sim, A.K. Wheatley, S.J. Kent, S.L. Hoffman, K.E. Lyke, P. Bejon, F. Luciani, K. Kedzierska, R.A. Seder, F.M. Ndungu, and I.A. Cockburn. 2021. Atypical B cells are part of an alternative lineage of B cells that participates in responses to vaccination and infection in humans. *Cell Rep* 34:108684.

Suurmond, J., and B. Diamond. 2015. Autoantibodies in systemic autoimmune diseases: specificity and pathogenicity. *J Clin Invest* 125:2194-2202.

Trautmann, A., M. Vivarelli, S. Samuel, D. Gipson, A. Sinha, F. Schaefer, N.K. Hui, O. Boyer, M.A. Saleem, L. Feltran, J. Müller-Deile, J.U. Becker, F. Cano, H. Xu, Y.N. Lim, W. Smoyer, I. Anochie, K. Nakanishi, E. Hodson, and D. Haffner. 2020. IPNA clinical practice recommendations for the diagnosis and management of children with steroid-resistant nephrotic syndrome. *Pediatr Nephrol* 35:1529-1561.

Tull, T.J., M.J. Pitcher, W. Guesdon, J.H.Y. Siu, C. Lebrero-Fernández, Y. Zhao, N. Petrov, S. Heck, R. Ellis, P. Dhami, U.D. Kadolsky, M. Kleeman, Y. Kamra, D.J. Fear, S. John, W. Jassem, R.W. Groves, J.D. Sanderson, M.G. Robson, D.P. D'Cruz, M. Bemark, and J. Spencer. 2021. Human marginal zone B cell development from early T2 progenitors. *J Exp Med* 218:

Vanderlugt, C.L., and S.D. Miller. 2002. Epitope spreading in immune-mediated diseases: implications for immunotherapy. *Nature Reviews Immunology* 2:85-95.

Vivarelli, M., K. Gibson, A. Sinha, and O. Boyer. 2023. Childhood nephrotic syndrome. *The Lancet* 402:809-824.

von Büdingen, H.C., T.C. Kuo, M. Sirota, C.J. van Belle, L. Apeltsin, J. Glanville, B.A. Cree, P.A. Gourraud, A. Schwartzburg, G. Huerta, D. Telman, P.D. Sundar, T. Casey, D.R. Cox, and S.L. Hauser. 2012. B cell exchange across the blood-brain barrier in multiple sclerosis. *J Clin Invest* 122:4533-4543.

Watts, A.J.B., K.H. Keller, G. Lerner, I. Rosales, A.B. Collins, M. Sekulic, S.S. Waikar, A. Chandraker, L.V. Riella, M.P. Alexander, J.P. Troost, J. Chen, D. Fermin, J.L. Yee, M.G. Sampson, L.H. Beck, J.M. Henderson, A. Greka, H.G. Rennke, and A. Weins. 2022. Discovery of Autoantibodies Targeting Nephrin in Minimal Change Disease Supports a Novel Autoimmune Etiology. *Journal of the American Society of Nephrology* 33:238.

Ye, J., N. Ma, T.L. Madden, and J.M. Ostell. 2013. IgBLAST: an immunoglobulin variable domain sequence analysis tool. *Nucleic Acids Research* 41:W34-W40.

Ye, Q., D.-J. Wang, B. Lan, and J.-H. Mao. 2023. T-cell and B-cell repertoire diversity are selectively skewed in children with idiopathic nephrotic syndrome revealed by high-throughput sequencing. *World Journal of Pediatrics* 19:273-282.

Zhou, J.Q., and S.H. Kleinstein. 2019. Cutting Edge: Ig H Chains Are Sufficient to Determine Most B Cell Clonal Relationships. *The Journal of Immunology* 203:1687-1692.